Utrecht University

Analogue modelling of extensional reactivation of thrust wedges

A MSc thesis by Javier Hidalgo

Supervisor: Dr. Ernst Willingshofer
Second supervisor: Kristóf Porkoláb

Research performed at the TecLab, Utrecht University
Faculty of Geoscience
Department of Earth Sciences

2019

ABSTRACT **4**

1. INTRODUCTION **5**

1.1. Inversion tectonics 5
1.2. Analogue and numerical models 5
1.3. Fundamentals of fault reactivation 7
1.4. State-of-the-art 9

2. METHODS **13**

2.1. Experimental set up 13
2.1.1. Series set up variations 15
2.2. Modelling strategy 16
2.3. Scaling 18
2.4. Materials 19
2.4.1. Brittle behaviour 19
2.4.2. Ductile behaviour 20
2.5. Monitoring / Data collection 22

3. RESULTS **24**

3.1. Series I 24
3.1.1. Compressional benchmark CBM2 24
3.1.2. NEG INV 4 24
3.1.3. NEG INV 10 27
3.2. Series II 29
3.2.1. Compressional benchmark CBM3 29
3.2.2. NEG INV 1 29
3.2.3. NEG INV 5 32
3.2.4. NEG INV 6 34
3.3. Series III 36
3.3.1. Compressional benchmark CBM1 36
3.3.2. NEG INV 7 36
3.3.3. NEG INV 9 39
3.3.4. NEG INV 8 41
3.4. Summary of modelling results 43

4. DISCUSSION **49**

4.1. Looking back at the state-of-the-art 49
4.2. Influences of tilting the system 49
4.3. Influences of frictional versus ductile decollements 49
4.4. Relevance of modelling results for natural examples 51
4.5. Future research 55

5. CONCLUSIONS **56**

6. ACKNOWLEDGEMENTS **57**

7. REFERENCES **58**

8. APPENDIX **60**

8.1. Developing the set up 60

ABSTRACT

Analogue modelling techniques are used to explore the reactivational behaviour of thrust wedges in extensional tectonic settings. Multiple experiments with distinct rheology's are tested under various conditions such as flat and tilted. Between these experiments, the reactivation behaviour of the pre-existing faults is compared to explore in what scenario reactivation is most dominant. A new modelling technique is developed where a rubber sheet is used to model extension, producing a homogeneously extended model. This extensional modelling is the second part of the experiment as negative inversion is modelled (shortening followed by extension). Previous researches have typically made use of a velocity discontinuity (VD), forcing extension to occur at a certain location in the model. As this thesis aims to explore the reactivational behaviour during a negative inversion tectonic setting, a VD would produce irrelevant results as the model is not free to react in the most energy favourable way.

Three experimental series are presented where i) makes use of solely brittle materials (quartz sand), ii) makes use of brittle materials which are quartz sand and (lower friction) glass beads and iii) makes use of both brittle and ductile materials (quartz sand and PDMS silicone putty). Each experimental series has a flat model and a 5º inclined model. Series ii and iii present an extra experiment where the effects of an extra low friction layer and a lower strain rate are explored respectively.

The experiments show that all experimental series adhere to the rule that tilting the system localizes deformation. Further, reactivation is only significant when a weak zone is present in the model. Series iii experiments demonstrate this by dragging silicone putty up in the model during shortening, along which during extension reactivation occurs. The model accommodate extension in two ways: i) By distributed extension that effects the entire model and ii) by localized deformation at pre-existing thrust contact or at the locations where new normal faults develop. Series i and ii demonstrate that (slight) reactivation is only visible by using particle tracing techniques and studying the relative strain rate variations during the experiments. The structures produced by series iii experiments have a high resemblance to naturally existing structures where the same interplay of (back) thrusts and (antithetic) normal faults is visibly in both the model and nature. Brittle/ductile models show that forward thrust become steeper during extension, as significant reactivation is occurring along a single plane. This causes large blocks to rotate whilst sliding down the reactivated contacts. The main conclusion of this thesis is that in order for extensional reactivation of thrust structures to occur, a weak area must be present within or below the thrust structure. If this is not the case, it will be energy favourable for the model to create new normal faults and accommodate extension that way. Future analogue modelling research on this topic should exclusively model brittle/ductile systems.

1. INTRODUCTION

1.1. Inversion tectonics

The term inversion is often used to describe distinct processes. In an attempt to clarify the use of the term, Cooper et al. (1989) presented a discussion where they concluded that the definition of inversion is a basin that is actively controlled by faults and that is infilled is subjected to a change in region stress system. This change results in the reactivation of pre-existing faults where the hanging wall is affected. Negative inversion, which this thesis aims to explore, is concluded to be shortening followed by extension.

1.2. Analogue and numerical models

Analogue modelling was instrumental for our understanding of the mechanical control on deformation on various length and time scales (Brun, 2002 and references therein). Within the vast spectrum of applications, the study of inversion structures has gained much attention, largely driven by the hydrocarbon industry, because these structures often form traps to oil or gas reservoirs. Consequently, the majority of investigations focused on the reactivation of extensional structures and the positive inversion of basins when compressed (McClay, 1989; Hu et al., 2017; Ventisette et al., 2006; Wang et al., 2017; Bonini et al., 2012). Much less attention has been devoted to the reactivation of contractional structures during subsequent extension of the crust, which is called negative inversion (Williams et al, 1989; Faccenna et al.,1995; Krantz, 1991; McClay, 1989) (Figure 1), yet this type of reactivation is documented from many mountain belts and thrust wedges including the Variscan mountain belt, the Dinarides or the Aegean domain (e.g. Huet et al., 2011; Stojadinovic et al., 2013; Ustaszewski et al., 2010; Bonev and Beccaletto, 2007).

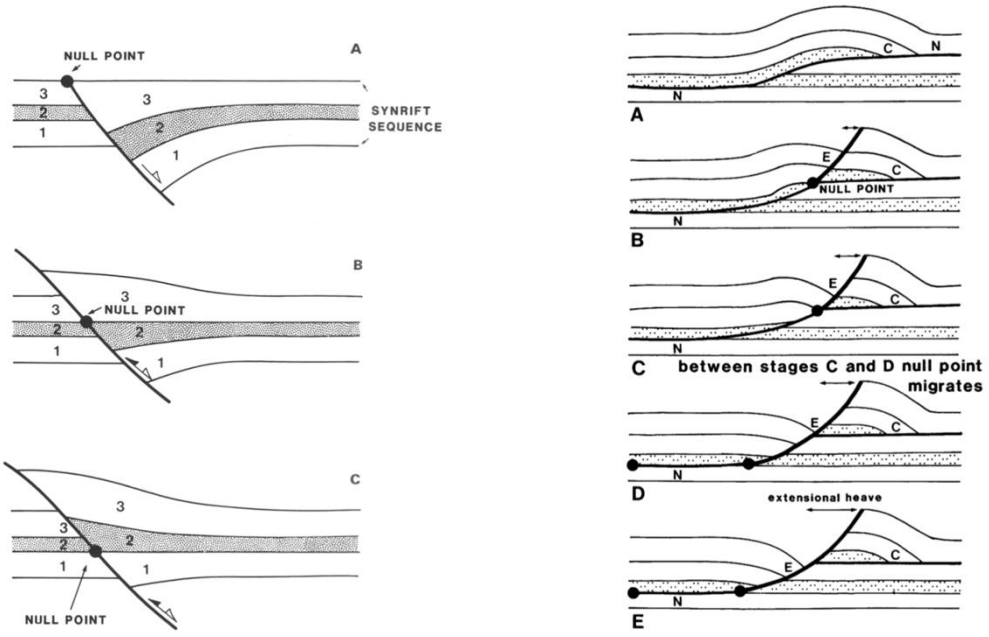

Figure 1: Sequential diagrams showing the contractional inversion of an extensional fault (l) and the shortcutting and partial reactivation of a thrust fault by extensional movements (r). Modified after Williams et al., (1989).

An example research that documents this tectonic process is the paper by Brun and Faccenna (2008). This paper described the exhumation of high grade metamorphic rocks as a result of slab rollback (Figure 2) in the Calabria-Apennine and the Aegean belts. The paper also described the resulting extensional reactivation of the nappe contacts. The figure illustrates the process of how material from the continental crust can be first shortened during subduction and later extended during slab rollback. The thrust structures that are shown in the compressional front (Figure 2b) are later reactivated. The image is a good visual aid in understanding the tectonic setting that is modelled in this thesis and provides insights in to why the results are to be considered as relevant.

An alternative technique to analogue modelling is numerical modelling where finite element models are used to model desired processes. Both modelling techniques have their appropriate pros and cons and some researchers have even published work where the two are compared head to head (e.g. Ellis et al. (2004)). They describe that both techniques show a distinct difference in brittle/ductile systems and brittle only systems. They show that for both types of systems the numerical models tend to produce thrust shear zones that are steeper than in the analogue models. It is argued by Ellis et al. (2004) that this is a result of numerical models using finite elements code that utilise a non-associated plasticity flow law. However, knowing this discrepancy exists and properly scaling the models, numerical models can still be used to model frictional materials. In this case the advantages of numerical models outweigh the possible disadvantages.

This thesis aims to explore strain localization (i.e. reactivation) during the negative inversion of a thrust wedge by applying the rubber-sheet technique to achieve uniform extension of a thrust wedge in analogue models. Exploring reactivational behaviour in a negative inversion tectonic setting using by applying uniform extension has never been done before.

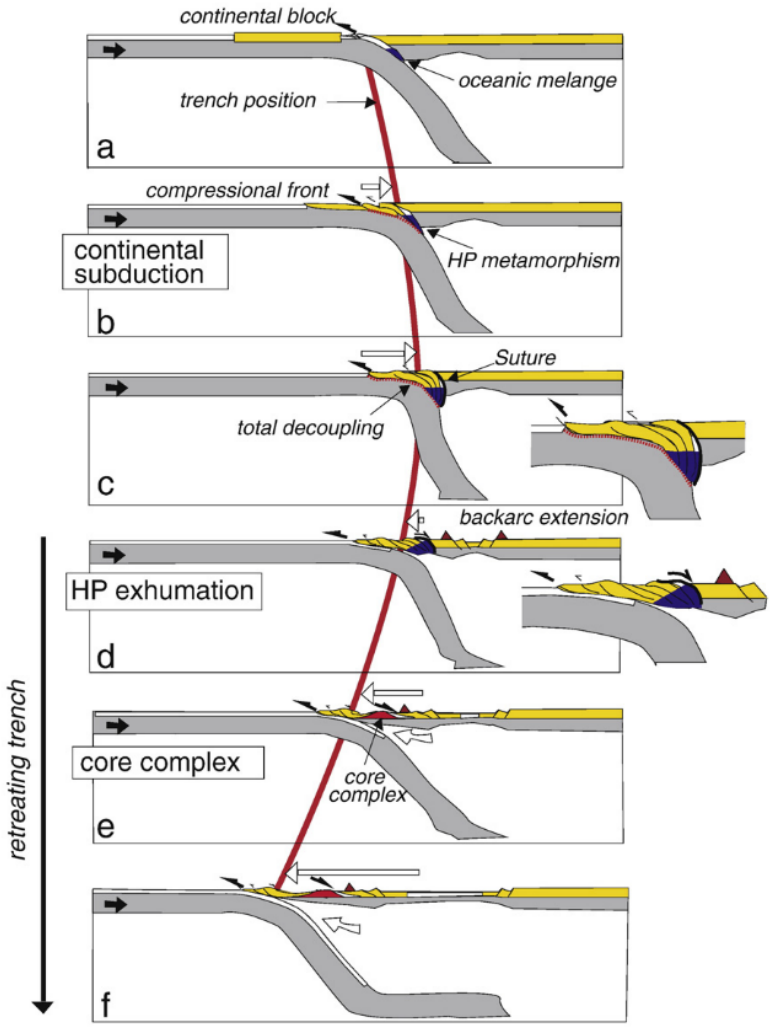

Figure 2: Schematic example of crustal material first being subjected by shortening (a, b and c) and later by extension (d, e and f) after slab rollback initiated. At the location of the suture zone (c) a magnification is visible where thrust structures are produced that are later reactivated in extension. Modified after Brun and Faccenna (2008).

1.3. Fundamentals of fault reactivation

Tectonic processes such as continental collision are often accommodated by the reactivation of existing structures rather than creating new structures (Sibson, 1985). It is important to understand what circumstances trigger reactivation and what parameter positively affect the plausibility of reactivation. Simply speaking a fault is reactivated when reactivating a fault requires less energy than creating a new fault. This fact is dependent on a few parameters which will be discussed.

The strength of a fault compared to its surrounding (unfaulted) areas is weaker than the surrounding rock. This is shown in Figure 3 where a Mohr-Coulomb circle is plotted with the failure envelopes of an unfaulted area and a fault that cuts through that area.

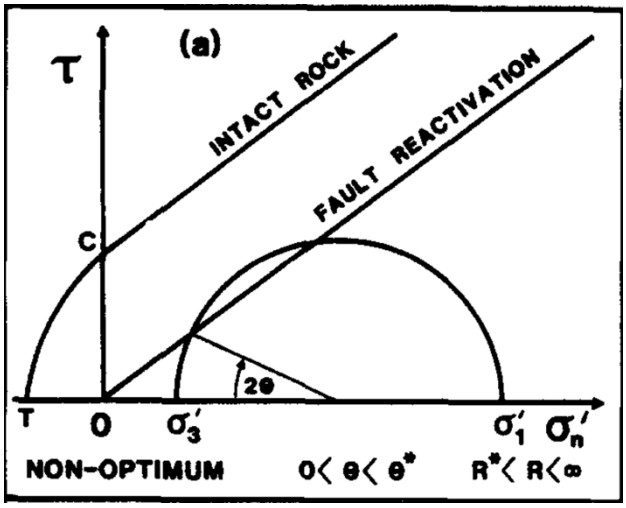

Figure 3: Mohr diagram showing the failure envelopes of intact rock and of a fault that runs through the rock. The Mohr circle, representing the strength of the rock, indicates that in this case the rock would be reactivated as the failure envelope of the fault is passed by the Mohr circle of the rock.

The image shows that in this situation, the fault would be reactivated as the strength of the fault is lower than the strength of intact rock. The Mohr circle that is visible exceed the failure envelope of the fault, but not that of the intact rock. Thus in this situation, less energy is required to reactivate the pre-existing structures than to create a new fault. The presence of pore fluid pressure effectively weakens the rock as the Mohr-circle is brought closer to the failure envelope. Cohesion differences (where the fault is lower than the surrounding areas) can also trigger reactivation of a fault.

The experiments in this thesis are not able to model parameters such as pore fluid pressure, therefore rheological differences are the cause of strength differences.

1.4. State-of-the-art

The studies by Faccenna et al. (1995), Krantz (1991) and Rosas et al. (2017) are considered to be of relevance as a state-of-the-art description for this research. The experimental set ups used by Faccenna et al. (1995) and Krantz (1991) are described in detail as these researches are similar to this thesis. The modelling approach used by Rosas et al. (2017) is different than this thesis (they use a rigid ramp, moreover later), whilst this thesis allows for the models to develop their proprietary ramps. However, the results of Rosas et al. (2017) are shortly touched upon.

The experiments performed by Faccenna et al. (1995) can be divided into two sets of experiments with distinct complexities. The first set uses solely dry quartz sand to model the brittle behaviour of the crust. The second set combine dry quartz sand with silicone putty in order to model both the brittle behaviour of the crust and the ductile behaviour of the decollement layer. Both sets of experiments use the same experimental set up where a mobile basal plate attached to a vertical backstop slide at a constant velocity (Figure 4). A velocity discontinuity (VD) is present at the base of the model. Shortening occurs at an angle relative to extension which is always perpendicular to the VD. The angles vary from 3º to 90º The duration of the models is determined by the first appearance of related faults. The main results are i) normal faults only slightly interact with shallow-dipping thrust faults by joining on their plane. ii) When pre-existing thrust faults have dip angles of 32° ± 1°, normal faults branch out from these faults at the decollement level. iii) reactivation of thrust faults as normal faults is dependent on the shear strength of the faults. The models show that extensional reactivation of thrust planes only occurs on thrust planes with dip angles larger than 41° ± 1°.

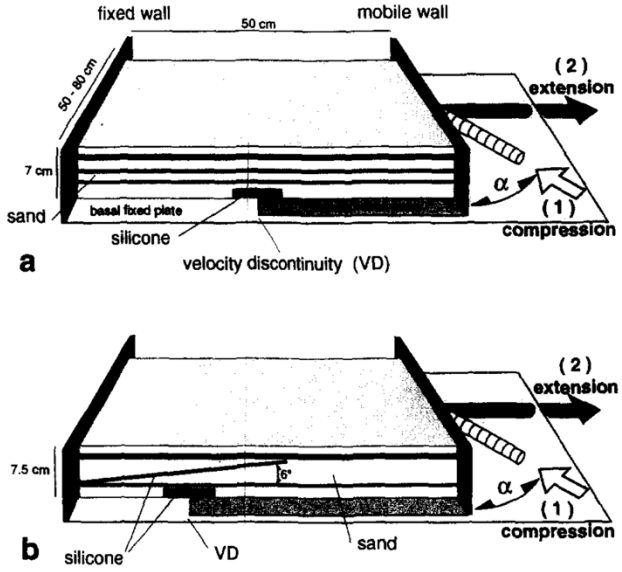

Figure 4: Experimental set up used during the experiments by Faccenna et al. (1995). Modified after Faccenna et al. (1995).

Krantz (1991) performed experiments solely using quartz sand. These experiments only represent the brittle behaviour of the crust. The experimental set up makes use of a basal VD beneath the layered sand (Figure 5). The boundary conditions of the set up consist of glass side walls treated with a hydrophobic coating. The amount of shortening is set at 5 cm, after which the box is tilted to various degrees (0°-20°, with 5° increments). This effectively increases the tilt of the pre-existing thrust planes. Next erosion is modelled using a vacuum cleaner. After the period of erosion new sediments are deposited using horizontal markers. Lastly, 5 cm of extension is

applied to the experiment in its tilted condition. Additionally, Krantz et al. (1991) performed an experiment that makes use of a rubber base. This results in the absence of a VD. The rubber base is fixed to the walls as to maintain a purely plane strain deformation model. For this experiment the deformation sequence was similar to the initial experiments that did make use of a VD.

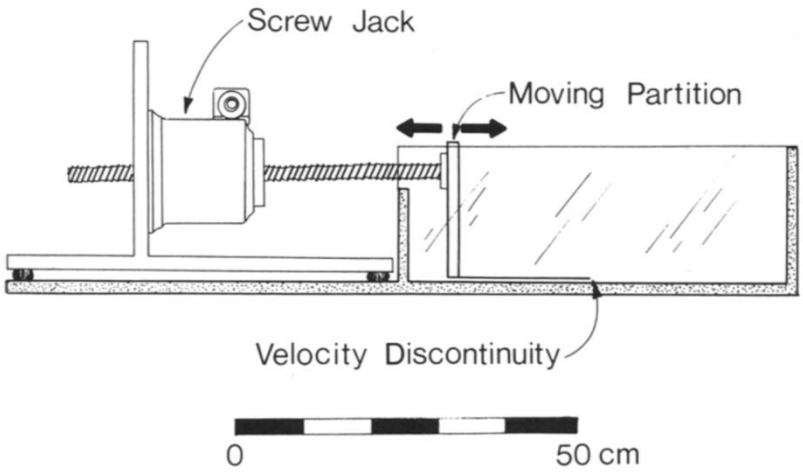

Figure 5: Experimental set up used by Krantz (1991). Modified after Krantz (1991).

The results of the experiments with VD show that faults that are dipping more than 40º are very likely to be reactivated during extension whilst faults that were dipping less than 40º were very unlikely to be reactivated. During early extension normal faults concentrated around areas with pre-existing thrust faults. During the final stages of the experiments were characterized by the development of new normal faults in undisturbed areas. The experiment performed with the use of a rubber base, showed that the development of thrust faults was different than previous experiments even though the experimental apparatus was similar. The thrust faults developed in no particular area in the model. Additionally, the faults all showed little displacement but significant horizontal axes rotation. Thrust faults developed at 25º-30º were rotated to 60º. During extension nearly all thrust faults were (partly) reactivated as new faults developed above the pre-existing structures. Deeper in the model these faults join on the planes of the pre-existing faults. An overview figure is given, schematically indicating the structures after compression and after compression and extension (Figure 6).

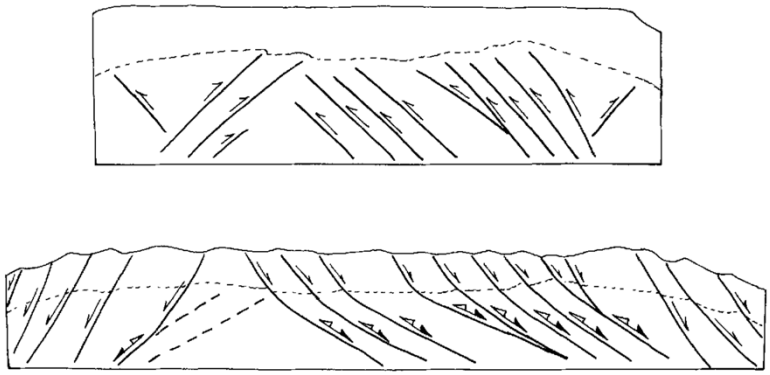

Figure 6: Schematic overprint of present structures after compression (top) and after compression and extension (bottom). Modified after Krantz (1991).

All available modelling parameters for the discussed researches above are given in Table 1.

Research paper	Experimental series	Kinematics / set up						Rheology							
		Presence of VD?	Base set up	Strain rate	Rotation	Length	Width	Brittle				Ductile			
								Material	Thickness	Material properties	Material	Thickness	Material properties	Interlayered putty
Faccenna et al. (1995)	Set I	Yes	Base plate attached to vertical backstop	Shortening: 1 cm/h Extension: 1 cm/h	n/a	50 cm	50 - 80 cm	Dry quartz sand	7 cm	ρ = 1.6 θ = 28°	n/a	n/a	n/a	n/a h = 0.5 cm ρ = 1.3 η = 10^{3} Pa s
	Set II	Yes	Base plate attached to vertical backstop	Shortening: 0.5 cm/h Extension: 0.25 cm/h	n/a	50 cm	50 - 80 cm	Dry quartz sand	7 cm	ρ = 1.6 θ = 28°	Silicone putty	1 cm	ρ = 1.4 η = 10^{4} Pa s	n/a
Analogue														
Krantz (1991)	Series i	Yes	Base plate attached to moving backstop	n/a	0 - 20° with 5° increments (towards hinterland)	20 - 60 cm	35 cm	Dry quartz sand	5 - 15 cm	n/a	n/a	n/a	n/a	n/a
	Series ii	No	Rubber base fixed to walls	n/a	n/a	20 - 60 cm	35 cm	Dry quartz sand	5 - 15 cm	n/a	n/a	n/a	n/a	n/a

Research paper	Experimental series	Additional sedimentation / erosion	Duration	Note
Faccenna et al. (1995)	Set I	After compression 1 cm sand is added	Experiments terminated at first sight of related faults	compression occurs at varying angles relative to extension
	Set II	After compression 1 cm sand is added	Experiments terminated at first sight of related faults	compression occurs at varying angles relative to extension
Analogue				
Krantz (1991)	Series i	Erosion of thrust belt with vaccuum Horizontal sedimentation before extension Sedimentation during extension	5 cm shortening 5 cm extension	
	Series ii	Erosion of thrust belt with vaccuum Horizontal sedimentation before extension Sedimentation during extension	5 cm shortening 5 cm extension	

Table 1: All relevant and available experimental parameter from the discussed researches.

Rosas et al. (2017) set out to investigate the difference in reactivation between sharp flat-ramp-flat (FRF) geometry thrust wedges vs. concave-convex (CC) geometry wedges. They did this by using a deformation box with a rigid ramp/flat part with predetermined FTF or CC shape (Figure 7).

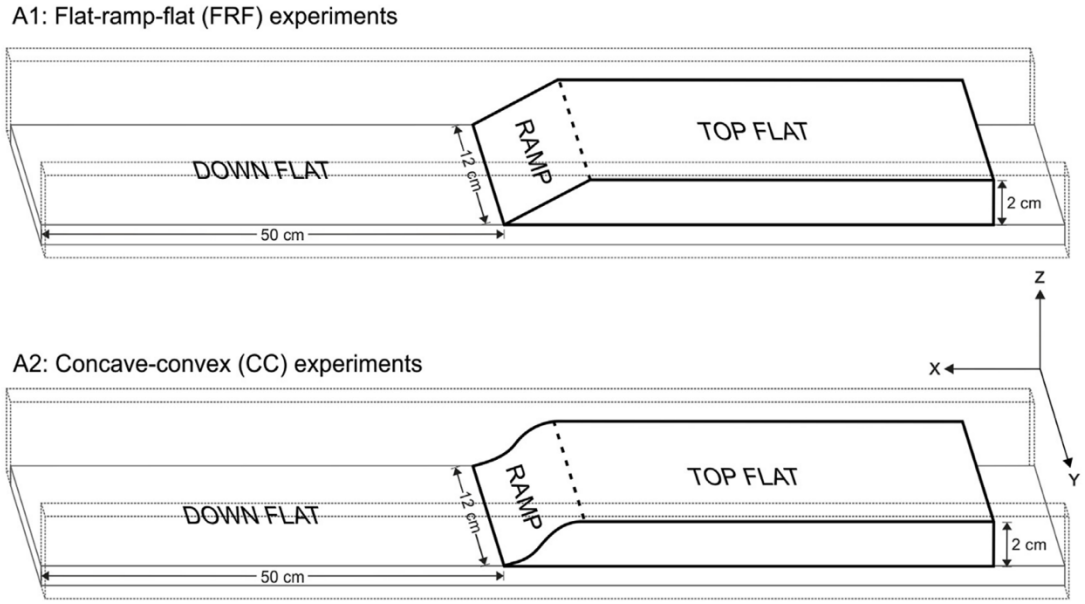

Figure 7: Perspex deformation box used for FTF and CC experiments. Modified after Rosas et al. (2017).

They found when an accretional wedge is sliding over the top flat part of an FTF wedge, changes in local stress are much more sharp than in CC wedges. High angle thrusts that formed over the top flat of FTF wedges are reactivated as normal faults during extension (Figure 8).

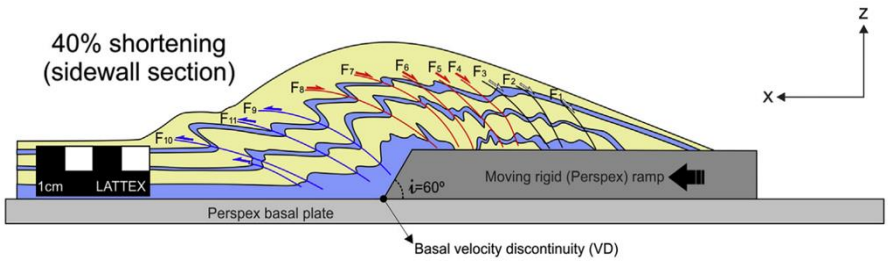

Figure 8: 60º RFR experiment at 40% shortening. Modified after Rosas et al. (2017).

2. METHODS

Analogue modelling had proven a valuable tool in studying natural processes occurring in the Earth's crust (e.g. McClay, 1989; Krantz, 1991; Jean-Pierre Brun, 2002; Hubbert, 1937; Schellart & Strak, 2016). The benefits of analogue modelling lie in the ability to study large scale processes occurring over long periods of time on a smaller scale and within a feasible period of time (days to weeks). This ability relies on scaling principles including geometry, kinematic and dynamic scaling (Brun, 2002).

2.1. Experimental set up

Traditionally a VD is used to determine where extension occurs (e.g. Faccenna et al., 1995; Krantz, 1991). This is a very effective and controlled way of modelling extension as the location of extension in the model is predetermined. The benefits of a VD are what make it undesirable in the experiments performed in this thesis. In this thesis it is not the goal to force extension to occur at the location of a thrust fault (by using a VD), but to determine what extensional accommodation occurs (i.e. what is the path of lowest energy). This is where the use of uniform extension becomes important as the entire model will be subjected to extension and the most energetically favourable way to accommodate extension will become apparent.

McClay (1989) set out to experiment with inversion using a rubber sheet as basal detachment, resulting in uniform extension (experimental series 1-3 in McClay, 1989). The aim of this set up was to examine the effects of inversion on domino style faults. Unfortunately, no clear figure or illustration was given to depict the set up. These experiments were split in 3 series with either different materials and/or different set up. Series 1 used homogeneous sand as modelling material whilst series 2 and 3 used alternating layers of sand and thin mica layers. Series 3 are experiments with a 5º tilt of basal detachment. The results of these experiments are similar. All series showed that only extensional faults shallower than 55º-60º were reactivated. Even when reactivated, the amount of displacement was limited. Reactivation movement ceased along a fault when the rotation had increased the faults to steeper angles.

As the objective of the experiments is to model the extensional reactivation of thrust wedges using uniform extension, a rubber sheet is used at the base. The sand model is built on a flat table on top of this rubber base, between metal bars, representing the side-walls to the experiments (Figure 9). The width of the rubber sheet and thus the model is 94 cm and the length is 68 cm. The thickness of the models are 1.6 cm.
Shortening is achieved by pushing a backstop between the bars. After shortening the model 15 cm, the backstop is detached from the engine. This allows the backstop to naturally move together with the thrust wedge during extension, which is 12 cm. Figure 9 shows a top view schematic overview of the set up. The rubber sheet is stretched from both sides by the same engine. This is achieved by routing the steel cable under the table. Multiple pulleys were used for this. The velocities of the models range from 1 – 15.08 cm/h depending on rheology and model.

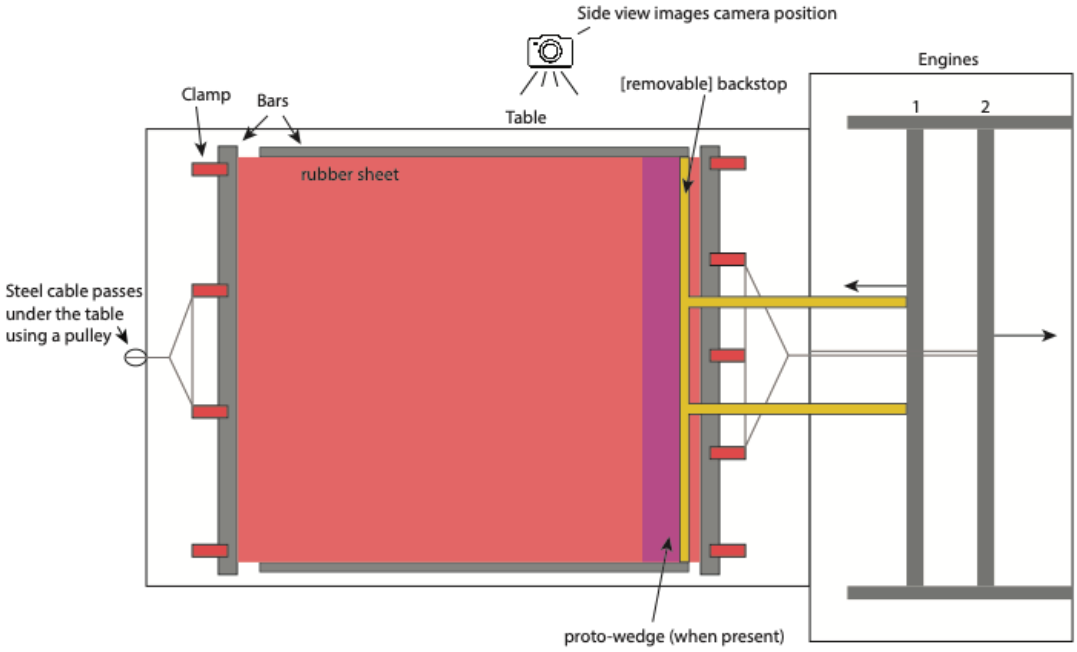

Figure 9: Schematic top view illustration of the experimental set up. Note the bars that are clamped over the entire width of the rubber sheet, properly distributing the pulling force.

The extensional kinematics are achieved by symmetrically pulling a rubber sheet. This rubber sheet allows uniform extension to be modelled, however because of the way rubber stretches, there will always be some unwanted contraction, perpendicular to the stretching direction (Figure 10 and Figure 11). For each experiment, digital image correlation techniques (DIC) have been applied (see 2.5 Monitoring / Data collection), which allows for mapping of the areas that have been affected by this contraction. For all models it is valid that the centre of the model is not affected by contraction. The size of this unaffected area is dependent on the width of the model where wider = larger unaffected area. For the width of the models presented in this thesis (94 cm), the unaffected area was about 5-8 cm.

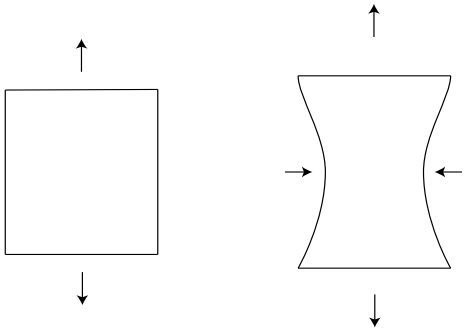

Figure 10: Schematic illustration of shortening occurring in the middle of a stretched rubber sheet. Note the shortening direction is perpendicular to the stretching direction.

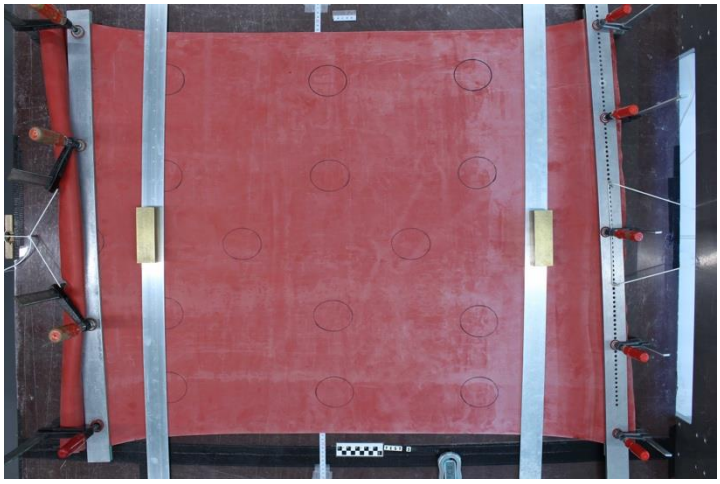

Figure 11: Top view image of Test 5 (a testing phase experiment aimed at exploring the behaviour of the rubber sheet) that shows the contraction of the rubber sheet perpendicular to the extension direction.

2.1.1. Series set up variations

This section will provide some information on the differences between the experimental set up of the series.

Series i contains experiments that only used quartz sand as modelling material. Figure 12 shows the initial cross sectional build-up of series i models

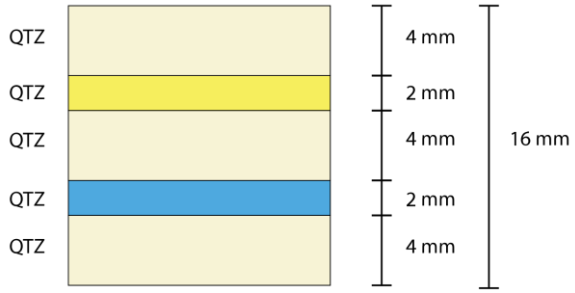

Figure 12: Initial cross sectional build-up of series i models. QTZ= quartz sand.

Series ii are experiments that have glass beads at the bottom of the model. The experiments are still only made up of brittle materials, namely quartz sand and glass beads. The materials have different rheological properties that translate in the glass beads (grainsize 100 - 200 μm) having lower friction than quartz sand. Inferred cohesion from glass beads can indicate near cohesionless Coulomb behaviour indicating that highly consistent and roundness may affect cohesion either by type of motion (rolling vs. sliding) or contact area (Klinkmüller et al., 2016). By using glass beads at the base of the models, the models have lower basal friction. Figure 13 shows the initial cross sectional build-up of NEG INV 1 and 5, Figure 14 shows the initial cross sectional build-up of NEG INV 6.

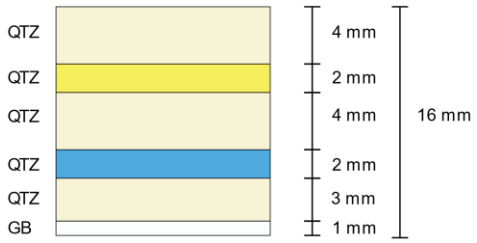

Figure 13: Initial cross sectional build-up of series ii models NEG INV 1 and NEG INV 5. QTZ= quartz sand, GB= glass beads.

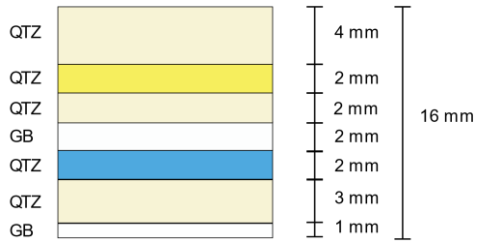

Figure 14: Initial cross sectional build-up of series ii model NEG INV 6. QTZ= quartz sand, GB= glass beads.

Series iii experiments are all brittle/ductile systems where a silicone putty base layer of 4 mm will be used instead of the base layer of 4 mm thick quartz that is used is series i and ii. This series will further investigate the influence of tilt (5º towards the hinterland) and strain rate. As described in section 2.4.2 Ductile behaviour of this thesis, the strength of silicone putty is increases with increasing strain rate. So e.g. a lower strain rate allows for a greater strength ratio between the ductile and brittle materials and vice versa. Another consequence of increasing the strain rate is the increased amount of coupling of the model. The strength ratios for NEG INV 7 are 3.2 during shortening and 1.1 during extension. For NEG INV 9 these are 3.2 and 1.1 respectively. For NEG INV 8 these are 16.0 and 5.3 respectively.
Figure 15 shows the initial cross sectional build-up of series iii models.

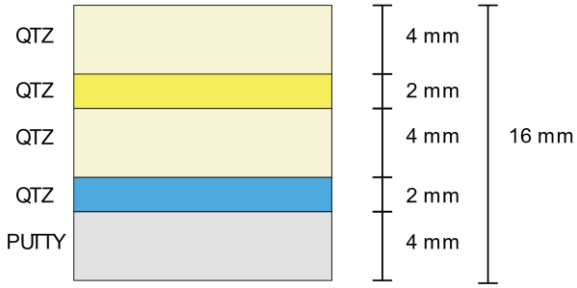

Figure 15: Initial cross sectional build-up of series iii models NEG INV 7, NEG INV 8 and NEG INV 9. QTZ= quartz sand, Putty= PDMS silicone putty.

2.2. Modelling strategy

In an attempt to better understand if and how a thrust wedge reactivates in extension a series of experiments is performed. These experiments will be grouped in 3 series where series

i. are experiments that use brittle materials only (quartz sand)
ii. are brittle only experiments that use glass beads at the base (quartz sand and glass beads)
iii. are experiments that have silicone putty at the base (quartz sand and silicone putty)

The experiments are split into series to try and distinguish between what parameters influence the reactivation of a thrust wedge. An overview of all experiments is given in Table 2. Figure 50 (page 46) shows an overview of all cross sectional interpretations that will be presented in this segment. The figure acts as a convenient way to compare results, eradicating the need for endlessly flipping pages/scrolling between sections. For the same reason, Figure 51 (page 47) is an overview figure of all the relative strain rate variations that will be presented in this thesis. At the beginning of the series sections a compressional benchmark will briefly be presented. These are (un tilted) models that have only been shortened 15 cm.

Series	Name	Length [cm]	Width [cm]	Thickness [cm]	Total compression [cm]	Total extension per side [cm]	Tilt	Velocity [cm/h]	Total runtime [hh:mm:ss]	Final thickness [mm]	Final width [mm]	Note
Series i	NEG INV 4	68	94	1.6	15	12	0º	15.08	01:45:53	39	206	-
	NEG INV 10	68	94	1.6	15	12	5º	15.08	01:46:02	44	109	-
Series ii	NEG INV 1	68	94	1.6	15	12	0º	15.08	01:46:18	43	190	-
	NEG INV 5	68	94	1.6	15	12	5º	15.08	01:46:34	43	149	-
	NEG INV 6	68	94	1.6	15	12	0º	15.08	01:45:44	44	153	Extra glass beads layer in the model
Series iii	NEG INV 7	68	94	1.6	15	12	0º	5	05:22:50	32	233	-
	NEG INV 9	68	94	1.6	15	12	5º	5	05:16:03	33	221	-
	NEG INV 8	68	94	1.6	15	12	0º	1	26:53:30	34	189	Lower strain rate

Table 2: Overview of all experiments and their experimental parameters. The results of total runtime, final maximum thickness and final width of deformation zone are also presented.

Figure 16 presents a legend that explains the annotations that will be seen in the figures presented in this thesis.

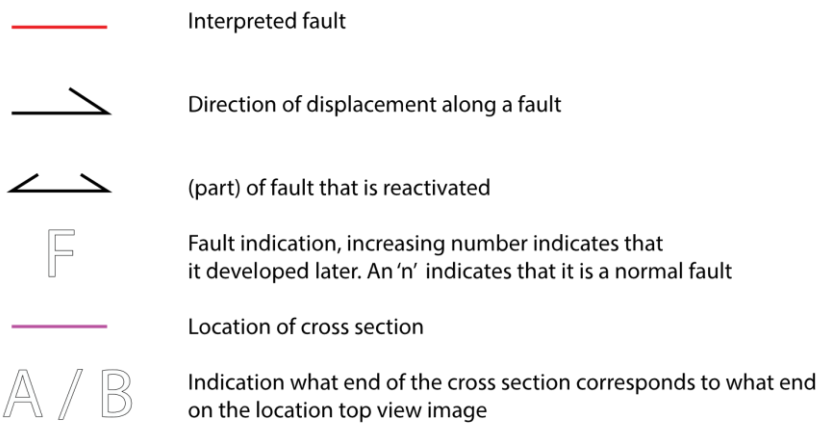

Figure 16: Legend of annotations that can be seen in the figures presented in this thesis.

The locations of the cross sections that will be presented are determined based on a vector field that is generated of the extensional phase of each individual experiment. One of such vector fields is shown in Figure 17 which is the vector field generator for experiment NEG INV 4. The image shows that the centre of the model is unaffected by the lateral contraction of the rubber sheet and that uniform extension is being modelled in the centre. The cross section through this centre will be interpreted and presented.

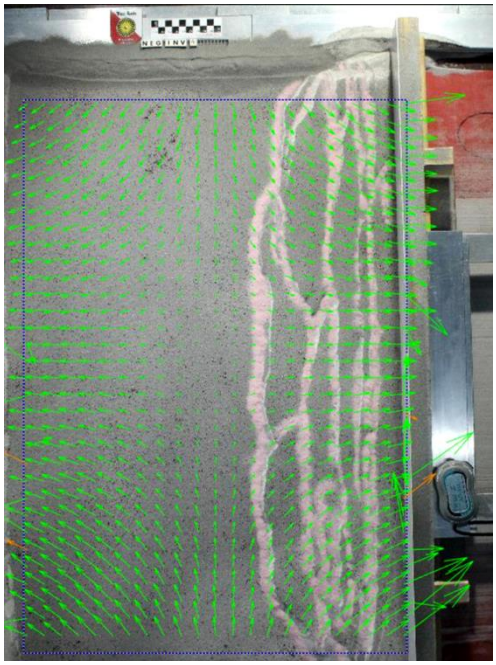

Figure 17: Displacement vectors during extension of NEG INV 4.

2.3. Scaling

The ability of comparing results between an analogue model to a natural phenomenon is dependent on the validity of said model. The model must correctly be scaled down in order to maintain the same strength ratio between different materials. The first scaling theory was published by Hubbert (1937) in the form of the theory of dynamic, geometric and kinematic similarities. Since the publishing of this theory, it has been used to study rock mechanics and geological structures. Scaling down a model means that parameters such as length, mass and time are correctly scaled to nature. IF done correctly, the average strength of brittle and ductile materials will be correctly scaled down according to each other and the gravitational forces. The dynamic equation for this is:

$$\frac{\delta\sigma_{ij}}{\delta x_{ij}} + \rho\left(g - \left(\frac{\delta^2\epsilon_{ij}}{\delta t^2}\right)\right) = 0 \qquad (eq.\,3.2.1)$$

where σ_{ij} are stress components, x_{ij} are space coordinates, ρ is density, g is gravitational acceleration, ε_{ij} are deformational components and t is time. Brun (2002) describes the following scaling relations

$$\sigma^* = \rho^* g^* L^* \qquad (eq.\,3.2.2)$$

$$\epsilon^* = g^*(t^*)^2 \qquad (eq.\,3.2.3)$$

with the exponent * being the model over nature ratio. Stress ratios (σ*), density ratios (ρ*), gravitational acceleration ratios (g*), length ratios (L*), strain component ratios ($\in$*) and time ratios (t*) are all relevant aspects of correctly scaling a model. Additionally, Hubbert (1937) shows that when studying geological processes, inertial forces can be ignored. This leaves us with equation 3.2.2. The experiments are performed at normal gravitational acceleration, giving $g^* = 1$. The density modelling materials have the same order of magnitude as the densities of natural

materials (see section 2.4. Materials below). This gives us $\rho^* \approx 1$. From this, Brun (2002) concluded that

$$\sigma^* = L^* \qquad (eq.\,3.2.4)$$

The set up used in this thesis models the top 10 km of the crust, thus 1 cm (model) = 6.25 km (nature).

2.4. Materials

The modelling materials used during the experiments are summarised in Table 3 below.

Material	Density ρ (kg/m^3)	Grain size (μm)	Grain shape	Viscosity η (Pas)	Coefficient of peak friction	Peak cohesion (pa)	n
Quartz sand	1500	100-355	rounded	x	0.626 (Willingshofer et al., 2018)	8.93 (Willingshofer et al., 2018)	x
Silicone putty (PDMS)	965	x	x	$1.49*10^4$	x	x	1 (Rudolf et al., 2016)
Glass beads	1530	100 – 200	spherical	x	0.478 (Klinkmüller et al., 2016)	10 (Klinkmüller et al., 2016)	x

Table 3: Material properties of model materials. Quartz sand and glass beads are used to model brittle behaviour and PDMS is used to model ductile behaviour. Coefficient of peak friction and peak cohesion are determined using the linear least-squares regression method.

Quartz sand and glass beads are used to model strong and weak brittle crust respectively. PDMS is used to model ductile behaviour.

2.4.1. Brittle behaviour

Brittle rocks in the Earth's crust deform in accordance with the Mohr-Coulomb criterion (Byerlee, 1978):

$$\tau = C + (tan\phi)\sigma \qquad (eq.\,3.3.1.1)$$

where τ represents the shear stress, C the cohesion, ϕ the angle of internal friction and σ the normal stress. The Mohr-Coulomb criterion also shows that the maximum differential stress of a brittle material linearly increases with depth, independent on strain rate. This maximum differential stress is

$$\sigma_1 - \sigma_3 = 2\rho g T_b \qquad (eq.\,3.3.1.2)$$

during compression, and

$$\sigma_1 - \sigma_3 = \frac{2}{3}\rho g T_b \qquad (eq.\,3.3.1.3)$$

during extension where σ_1 and σ_2 are maximum and minimum principle stresses and T_b is the thickness of the brittle layer. These formula's describe a time independent behaviour as no

formula has a time/rate component. This enables brittle only experiments to be ran at high strain rates.

2.4.2. Ductile behaviour

The power law equation

$$\dot{\epsilon} = Aexp(-\frac{Q}{RT})(\sigma_1 - \sigma_3)^n \qquad (eq.\ 3.3.2.1)$$

as described by Goetze and Evans (1979) allows to describe the flow of rocks in nature. In this equation $\dot{\epsilon}$ is the deviatoric strain rate, A is a material constant, Q is the activation energy, R is the universal gas constant, T is the temperature and the exponent n is the stress component.

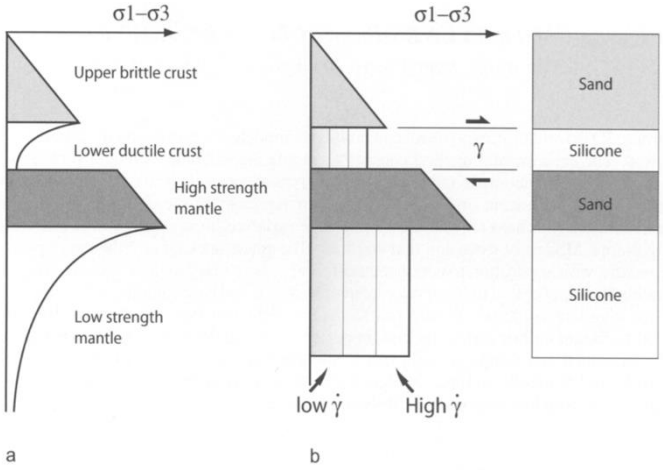

Figure 18: Simplification and replication of the strength profile of the crust. Where (a) is a strength profile of a natural system and (b) is the strength profile of a model made up of alternating sand and silicone layers. Modified after Brun (2002).

The silicone putty used to model ductile behaviour is a Newtonian fluid whose resistance to flow is directly linked to the strain rate (Brun, 2002)(Figure 18). The shear strain rate $\dot{\gamma}$ of silicone putty is

$$\dot{\gamma} = \frac{V}{T_d} \qquad (eq.\ 3.3.2.1)$$

where V is velocity and T_d is the thickness of the ductile layer. From equation 3.3.2.1 the shear stress of a ductile material can be described as

$$\tau = \frac{\eta V}{T_d} \qquad (eq.\ 3.3.2.2)$$

Or,

$$\tau = \eta\dot{\epsilon} \qquad (eq.\ 3.3.2.3)$$

Where η is the viscosity of the material. In terms of differential stress this can be written as,

$$\sigma_1 - \sigma_3 = 2\tau \qquad (eq.\ 3.3.2.4)$$

Using both the brittle and ductile differential stress definitions, strength profiles are constructed for the experiments. Varying certain parameters, namely thickness and strain rate, different types of strength profiles can be modelled. The application of a correct strength profile is crucial to the model being representative, as shown in Figure 18. Varying these parameters, i.e. the strength ratio's also changes the amount of coupling between rheologically distinct layers of the model (J.-P. Brun, 2002). High strain rate results in high ductile strength which in turn leads to high coupling. Below the strength profiles of the brittle/ductile experiments will be shown (Figure 19, Figure 20 and Figure 21).

The strength profile of NEG INV 7 (Figure 19) shows that during both phases of the experiment, the silicone putty was weaker than the quartz sand. However, it is important to note that during compression the quartz was significantly stronger (219% increase) than the putty whilst during extension the sand is only slightly stronger (7% increase) than the putty. This has to do with the fact that the differential strength of silicone putty is not dependent on the type of deformation (compression/extension) whilst the quartz sand is not.
The strength profile for experiment NEG INV 9 is visible in Figure 20. The figure shows that the quartz sand is stronger both during shortening and during extension. The strength profile and insights are the same as NEG INV 7.
The strength profile for experiment NEG INV 8 is visible in Figure 21. The figure shows that the quartz sand is stronger both during shortening and during extension. During shortening the sand shows a 1500% strength increase, during extension this increase is 433%. During both deformational phases the silicone putty is clearly much weaker.

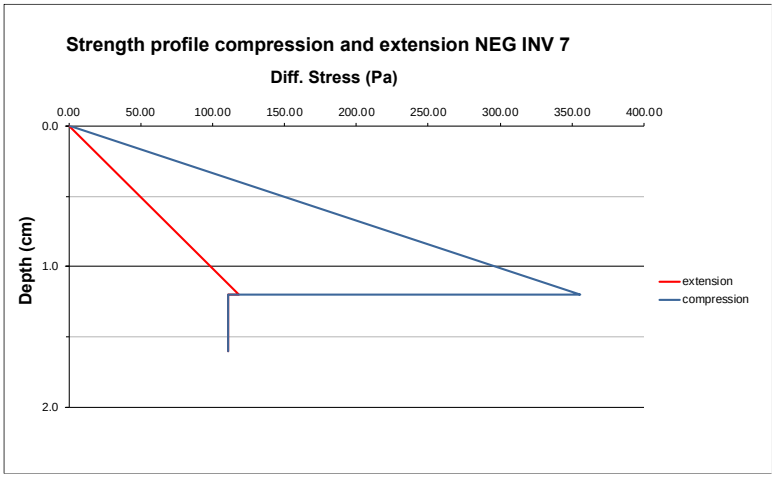

Figure 19: Strength profile of experiment NEG INV 7 showing the strength both during compression and extension. During both phases the strength of the silicone putty is the same, thus deeper than 1.2 cm the strength profile lines collide and are shown as one. Strength ratio during shortening = 3.2, strength ratio during extension = 1.1.

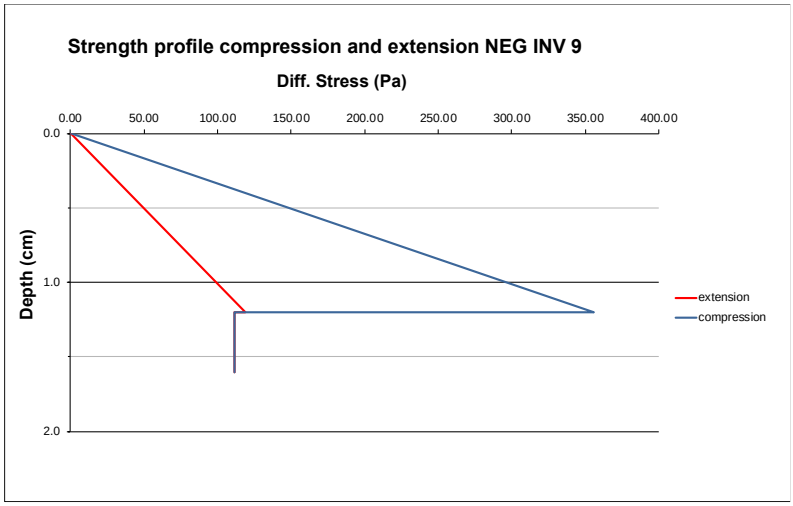

Figure 20: Strength profile of experiment NEG INV 9 showing the strength both during compression and extension. During both phases the strength of the silicone putty is the same, thus deeper than 1.2 cm the strength profile lines collide and are shown as one. Strength ratio during shortening = 3.2, strength ratio during extension = 1.1.

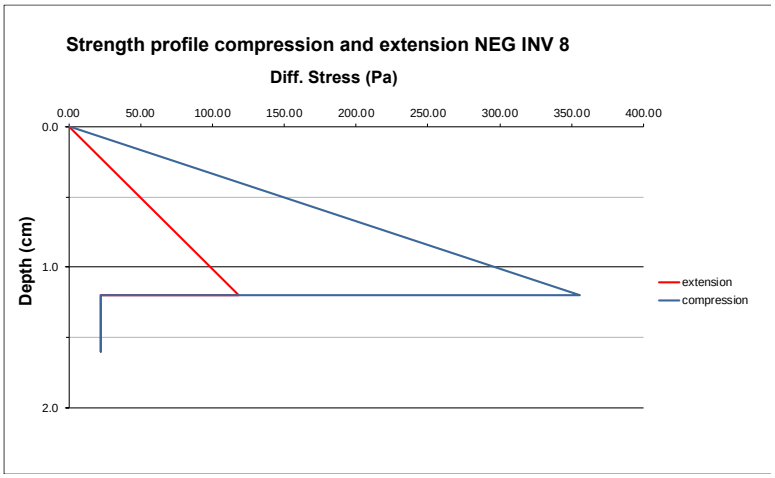

Figure 21: Strength profile of experiment NEG INV 8 showing the strength both during compression and extension. During both phases the strength of the silicone putty is the same, thus deeper than 1.2 cm the strength profile lines collide and are shown as one. Strength ratio during shortening = 16.0, strength ratio during extension = 5.3.

2.5. Monitoring / Data collection

The experiments presented in this thesis are monitored by taking photographs from multiple directions at set intervals, including top and side view imaging. Side view photographs are not horizontal but look at the model at an angle. These perspectives give the researcher the possibility to look at the development of the model from a natural viewpoint, as if standing next to it. After the model has been completed, the researches can replay the development of the model at whichever desired speed. Unfortunately no data can be collected from the side-view images (e.g. measure angles, heights etc.) as they are not square to the model. All image sequences are later combined into time lapse videos to get a better understanding of the development of the model.

On the top surface of the models, coffee grounds are sprinkled. These coffee grounds serve as trackable pixels for vector deformational analyses and relative strain rate variation analyses using PIVlab (DIC) (Thielicke & Stamhuis, 2014). PIVlab works by loading a series of images into the program with a constant timestep. The program then analyses each pixel in a predetermined "region of interest". For each consecutive image the program examines if the pixel has shifted and by how much. This PIVlab pixel particle analysis is a necessary aid to distinguish the slightest differences in strain rates that are undetectable by the naked eye, even when studying time lapse videos. Additionally, it provides data to verify if and where pure homogenous extension occurs above the rubber sheet (i.e. where the perpendicular contraction of the rubber relative to the extension direction has no effect on the model, further information in Figure 10 and Figure 11).
After the experiments terminated, the models are wetted and cut. Cross section images are taken using a camera and a black backdrop.

3. RESULTS

3.1. Series i

Series i contains experiments that only used quartz sand as modelling material.

3.1.1. Compressional benchmark CBM2

The structures produces by the compressional benchmark of series i is shown in Figure 22.

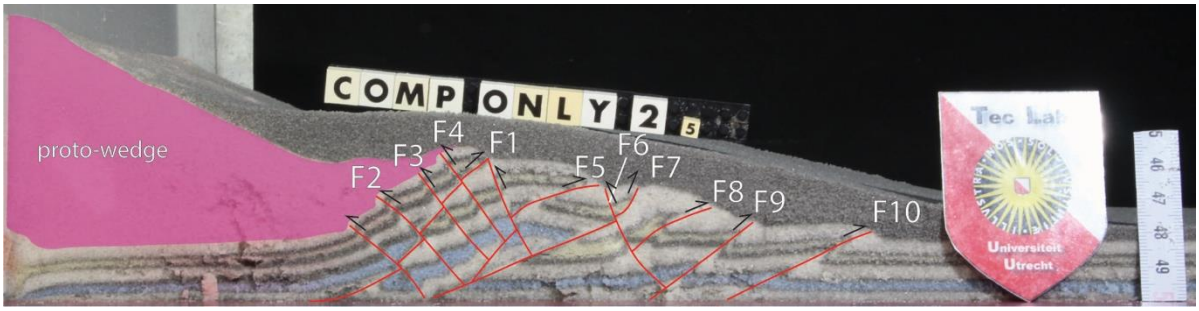

Figure 22: Cross section of the compressional benchmark for series i.

The wedge evolves by first developing a single forward thrust and 4 back thrusts (of which 3 can be timed) near the tip of the proto-wedge (more info on the proto-wedge in 3.2.2 NEG INV 1). Later, more forward thrusts develop in sequence from the backstop with one backstop in between (F6). The angles of all these faults are shown below in Table 4.

CBM2	angle [º]
F1	68
F2	45
F3	51
F4	53
F5	14
F6	66
F7	58
F8	22
F9	38
F10	24

Table 4: Angles of faults in the compressional benchmark of series i.

3.1.2. NEG INV 4

The thrust wedge evolves by initially developing a forward thrust close to the backstop. As shortening continues, three pop-up structures develop. First closer to the backstop and thereafter increasingly further away from the backstop.

Figure 23 is a top view image of the model after compression. The width of the deformation zone after shortening is 16.9 cm. The location of the cross section and relative strain rate variations during the final stages of extension can be seen in Figure 24. The strain rate variation shows that F1/F2 are reactivated during extension, but their displacement is still reverse as shown in Figure 25. The total width of the deformation zone is 20.6 cm after extension. Final maximum thickness of the model after completion is 39 mm. Figure 25 shows cross section 5 of the model after completion.

Figure 25 indicates that this experimental set up produces a fairly complex thrust system. Multiple pop-up structures are visible. Deformation initiates by developing multiple smaller thrust faults close to the backstop (F1,2,3) that produce ~ 8 mm displacement. Whilst shortening continues, faults with larger displacements (~36 mm) develop in sequence (F4,5,6) towards the foreland. All layers are thinned by 10% on average. This was determined by performing a pixel to length analyses of the cross section. As extension is not accommodated by the development of new normal faults of by reactivating existing thrust structures, it is accommodated by gradually thinning all layers. This is a result of the rubber sheet stretching out the model. This causes rotation of the thrust faults over the horizontal axis (F3: 19º, F6: 21º, F7: 16º), as they are incorporated in the thinning process.

The markers along the faults visible in Figure 25 indicate that even after extension, all faults are still reverse faults. No reactivation movement is visible along the faults as the distinctly coloured layers still show reverse offset. However, the particle tracing analysis also produced a strain rate variation image (Figure 24) which indicates that there is a slightly elevated strain rate along structures produced during compression. This indicates that the slightest reactivation does occur during extension. Important to note is that this strain rate analysis is from the early stage of extension. As extension progresses, increasingly less relative strain rate variation is visible throughout the model. This indicates that the reactivation is only occurring at the beginning of extension.

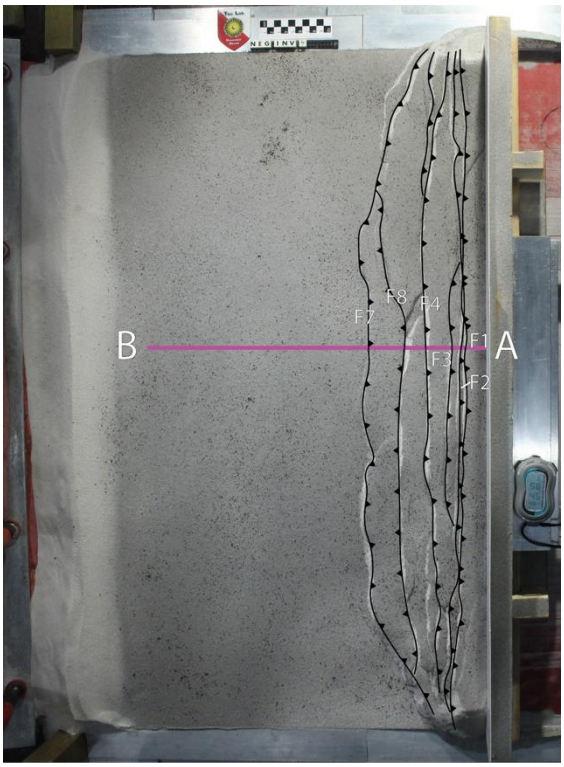

Figure 23: Top view image of the thrust wedge after completion of the shortening phase but before extension initiated.

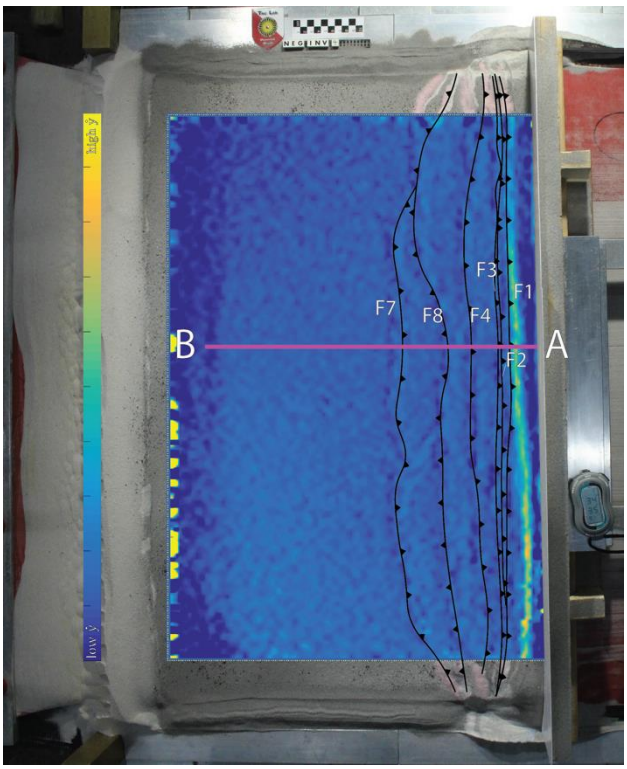

Figure 24: Relative strain rate variations during final stages of extension of NEG INV 4.

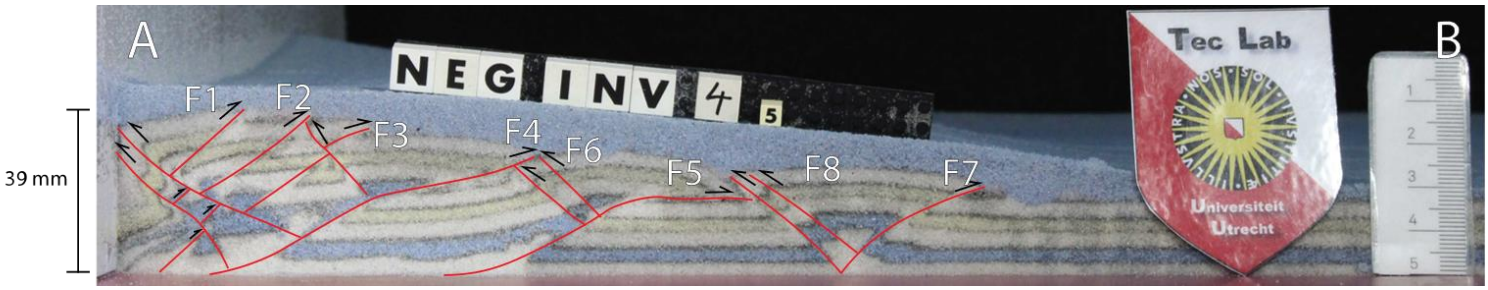

Figure 25: Cross sectional view and interpretation of NEG INV 4 cross section 5.

3.1.3. NEG INV 10

The aim of this experiment is to test the effects of a 5º tilt on the reactivation of a thrust wedge. Figure 26 shows a top view image of the model after shortening finished. At the start of shortening, quickly 3 forward thrusts developed. After these faults developed, shortening is accommodated by displacement along these contacts before a new fault is created. The width of the deformation zone after shortening is 10.8 cm. Figure 27 shows the location of the cross section in the model after extension including the strain rate variations during the final stages of extension. The width of the deformation zone is 10.9 cm after extension (47.1% decrease in width with respect to the un-tilted experiment). No thinning of the unfaulted layers is visible but a normal fault is visible close to the backstop. The final maximum height is 44 mm after completion of the model. Figure 28 shows the cross sectional analysis of cross section 4 through NEG INV 10. The model evolves by producing multiple thrust faults close to each other. Three of these faults (F1,2,3) are near parallel and have low angles (9º – 14º). These faults are all cut by the same, higher angle normal fault (Fn). This normal fault shows a steeper geometry than the thrust faults at 52º. One fault (F6) shows ramp / flat geometry. During extension a normal fault developed close to the backstop (Fn). This is the only visible fault that has a normal displacement (8 mm offset). All other faults still have a visible reverse displacement. Figure 27 shows the strain rate variations based on the particle analysis. This figure shows that the relative highest strain rate during extension is at the backstop. The previously formed thrust faults show slight higher strain rates than undeformed parts of the model. This indicates that even though it is not visible in the cross section (due to reverse displacement), the thrusts are slightly reactivated. But it is important to note that Figure 27 is from the early stages of extension. As in the early stages of extension a slight increase in relative strain rate is visible along the pre-existing thrust structures. As extension progresses, this elevated strain rate (i.e. reactivation of the thrust structures) becomes less and less to the point where no variation is visible.

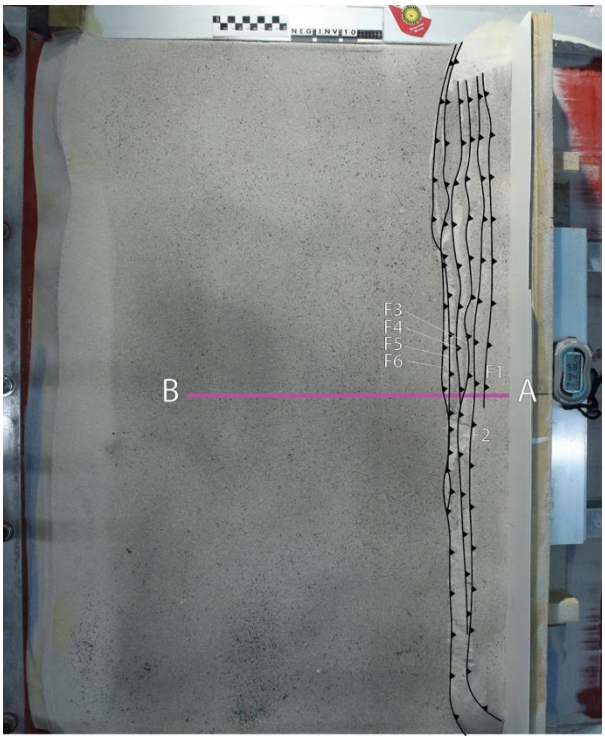

Figure 26: Top view image of model NEG INV 10 after shortening completed.

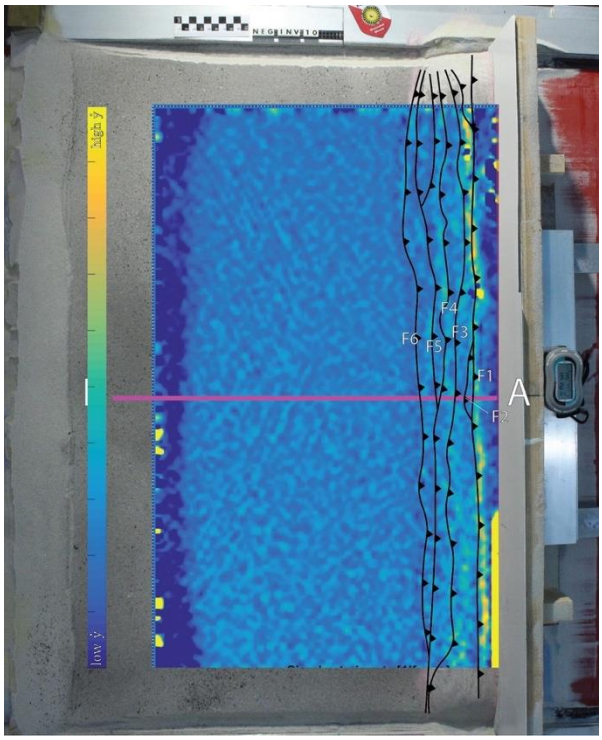

Figure 27: Relative strain rate variations during extension of NEG INV 10 based on the particle analysis. The relatively highest strain rates are visible at the location where the normal fault is visible in the cross section.

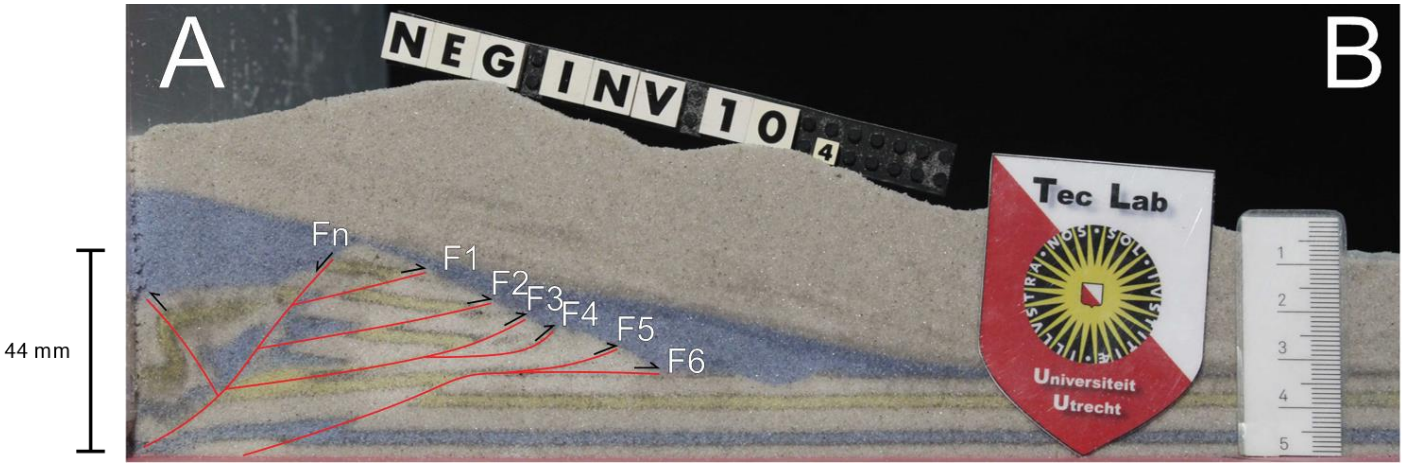

Figure 28: Cross sectional interpretation of cross section 4 through NEG INV 10.

3.2. Series ii

Series ii are experiments that have glass beads at the bottom of the model.

3.2.1. Compressional benchmark CBM3

Figure 29 shows the compressional benchmark for series ii experiments. The model has a low friction decollement made up of glass beads.

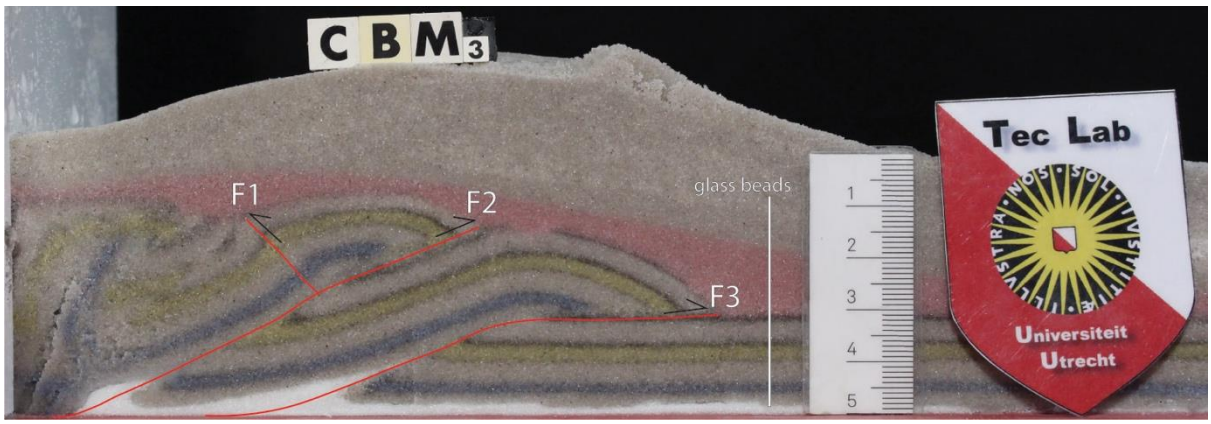

Figure 29: Compressional benchmark for series ii experiments.

The wedge evolved by first developing a back thrust close to the backstop. Later two large forward thrusts develop that have large amounts of displacement (F2: 3.8 cm and F3: 4.6 cm). Table 5 shows the angels of the faults above.

CBM3	angle [º]
F1	46
F2	22
F3	21

Table 5: Angles corresponding to the faults of the compressional benchmark of series ii experiments. Note that the angle of F3 corresponds to the "ramp" part of the fault.

3.2.2. NEG INV 1

This experiment has a 1 mm layer of glass beads at the base. The thickness of the model remains the same at 1.6 cm. This experiment made use of a proto-wedge. Extensive testing showed that this proto-wedge only shifts the deformation further from the backstop, no other changes are observed. This argument is used to place NEG INV 1 in series ii even though this discrepancy exists.

During shortening the model quickly develops a pop-up structure and a forward thrust. After these develop shortening is accommodated over the "flat" part of a forward thrust (F5, Figure 32). After which the structures further from the backstop develop in sequence. A top view image of the model after shortening is presented in Figure 30. A top view image after extension completed is shown in Figure 31. This figure also shows the location of cross section 5 through NEG INV 1 and shows a relative strain rate variation plot during final stages of extension. At no point during extension can any strain rate variations be observed.

The interpreted cross section of NEG INV 1 is depicted in Figure 32. Four main large thrusts formed during the experiment (F1,3,5,6). F1,3,6 ultimately result in the development of a pop up structure where the height of the topography decreases with increasing distance from the backstop. Three back thrusts are visible that are part of a pop up structure (F2,4,7) and a single back thrust is visible that is not associated with a pop up structure (Fb). These thrust structures start of as pop-up structures but most of the displacement is accommodated along the fore-thrusts. Thinning of the deposited layers is visible, which results in the rotation of F2 by 17º during the extensional phase. The other faults do not show any rotation compared to the compressional benchmark. The thinning is visible exceptionally well to the left of ''Fb'' where the blue and yellow layers are severely thinned.
No normal faults are visible that might have developed during the extensional phase. The final maximum thickness of the model is 43 mm which is an 169% increase from the initial thickness. The final width of the deformation zone is 10.9 cm. No thinning is measured outside of the deformation zone (at the location where the teclab logo is situated in Figure 32).

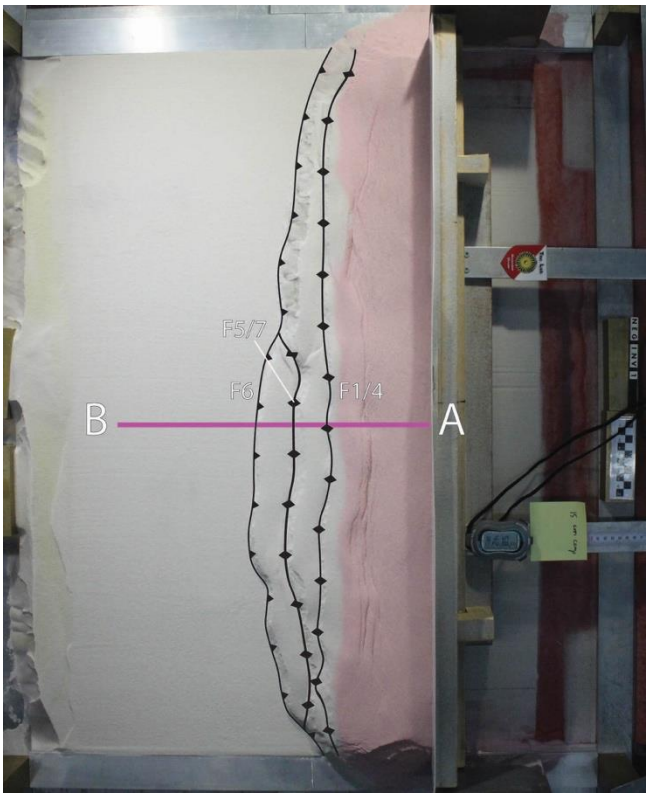

Figure 30: Top view image of NEG INV 1 after shortening. Structures and location of cross section 5 are shown.

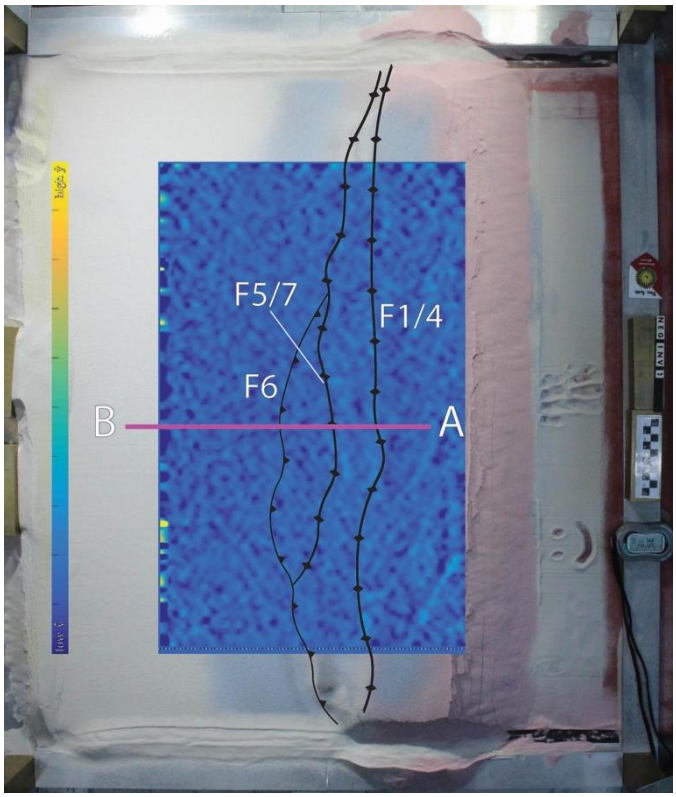

Figure 31: Relative strain rate variations during extension of NEG INV 1. Structures and location of cross section 5 are shown.

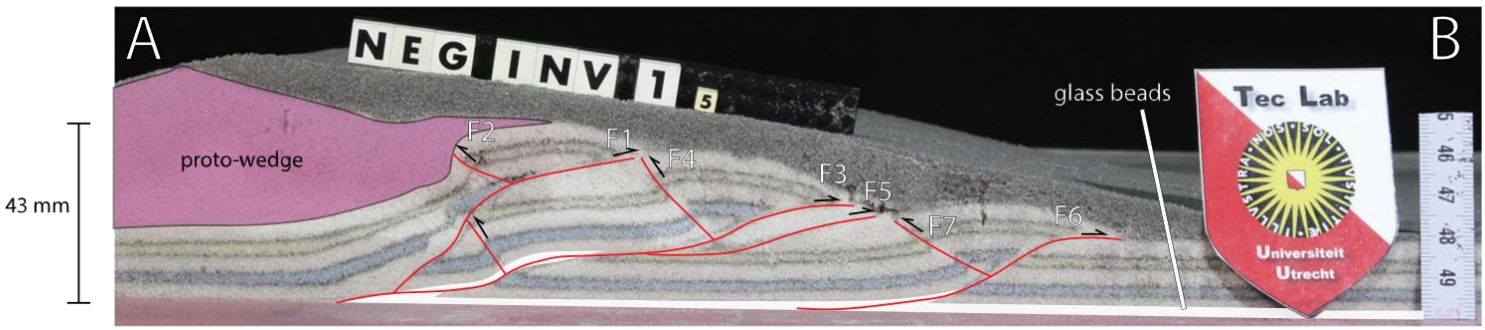

Figure 32: Cross section 5 and interpretation of structures of NEG INV 1.

3.2.3. NEG INV 5

This experiments aim to investigate the effects of combining a low friction base layer of glass beads with a 5º inclination towards the hinterland. The thrust wedge developed by first forming three forward thrust faults. After these formed, two more forward thrusts formed over which a lot of shortening was accommodated. The width of the deformation zone after shortening is 11.6 cm.

The interpreted cross section (Figure 35) shows the development of three rotated thrust faults (F1,2,3) and the later development of two lower angle thrust faults (F4,6). F4 ultimately produces a pop up structure. F6 develops a small fold in the hanging wall and shows a ramp/flat geometry. F1 is the first thrust fault to develop. After the compressional phase (Figure 33), the extension causes a normal fault to develop next to it with an origin at the same location as the end of the thrust fault. This normal fault is the main accommodation structure of the extension. This observation is backed by the strain rate variation visible in Figure 34 that indicates that the highest strain rates are present at the location of the normal fault. The amount of strain rate variation increased with time as the model evolved.
The blue layer shows severe thinning. No clear structures are visible to determine what causes this thinning. The final maximum height and width of the deformation zone are 43 mm and 14.9 cm respectively (a 21.6% decrease in deformation zone width with respect to the un-tilted experiment). A 5% thinning of the layers is visible in the model, measured by performing a pixel to length analysis.

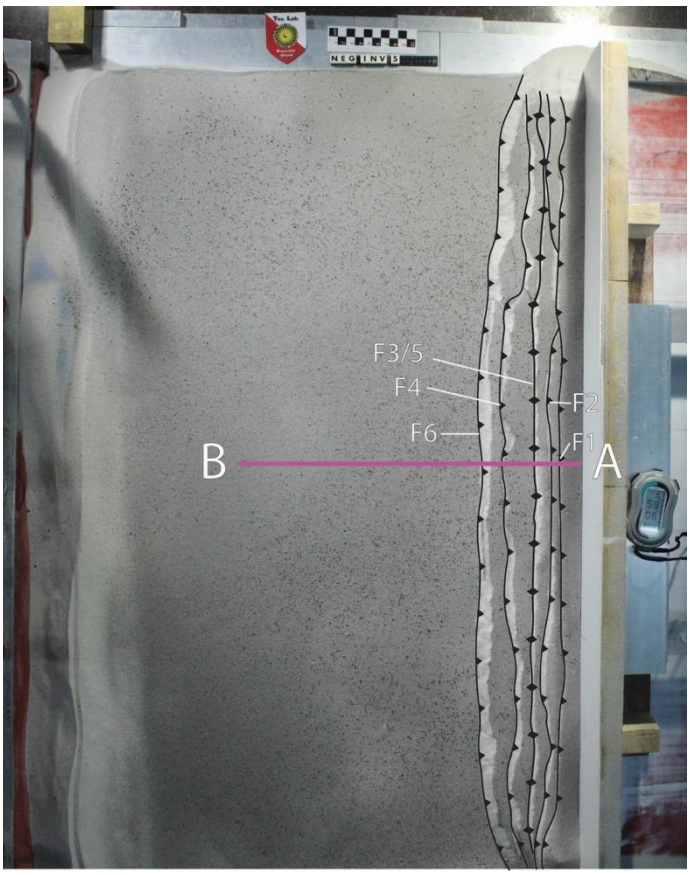

Figure 33: Top view image of NEG INV 5 after shortening completed.

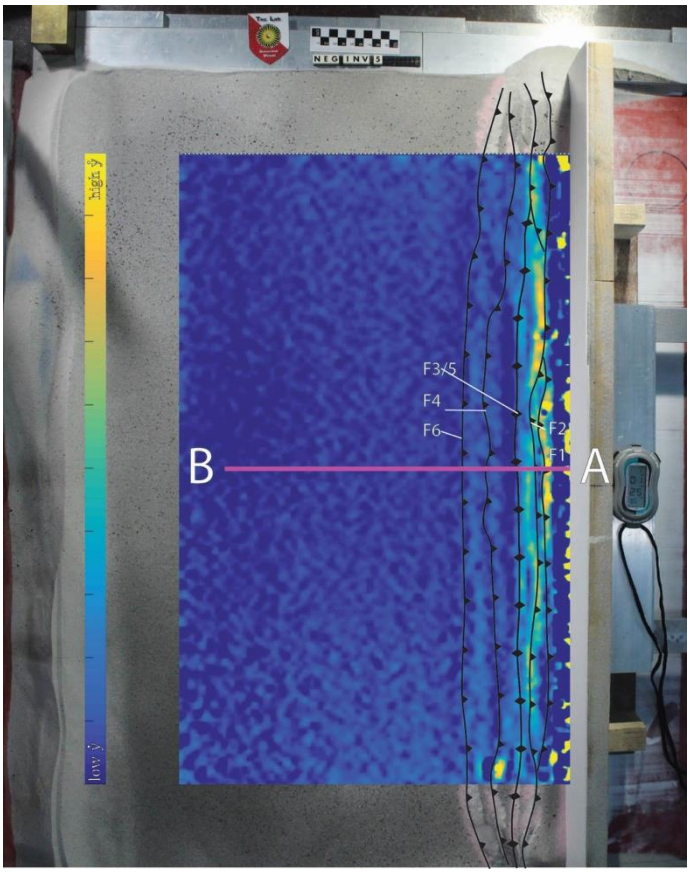

Figure 34: Relative strain rate variations projected on top of NEG INV 5. It is visible that close to the backstop at the location where the normal fault develops (close to F1, see cross section), the strain rate is highest. The location of the cross section through the model is also visible.

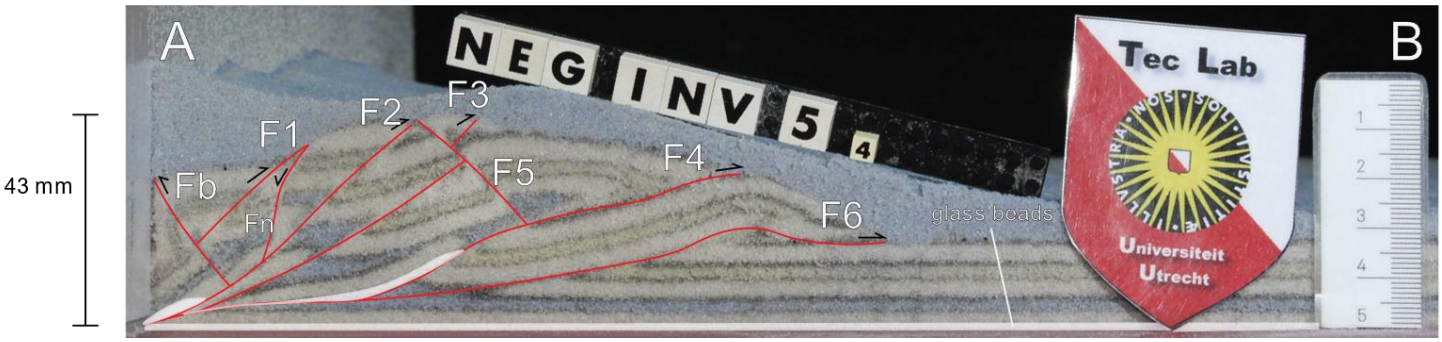

Figure 35: Cross sectional interpretation of cross section 4 cut through model NEG INV 5.

3.2.4. NEG INV 6

The objective of NEG INV 6 was to investigate the influence of a low friction layer in the middle of the model in addition to the low friction base. This was achieved by substituting 2 mm of quartz sand by 2 mm of glass beads.

The model evolved by first developing multiple small scale forward thrusts (F1,2,3). Later, larger thrusts developed (F5,7) that both resulted in a back thrust and pop-up like structure. F7,8,9,10 all branch from the same low angle thrust plane that has a large ramp / flat geometry. Figure 36 shows a top-view image of NEG INV 6 after shortening completed. The width of the deformation zone after shortening is 12.6 cm.

This model shows that extension was (partly) accommodated by the development of a normal fault (Fn). This fault is the only fault that shows normal movement based displacement. When studying the strain rate variation (Figure 37), it is confirmed that Fn accommodates most of the extension, whilst there is no significant strain rate variation throughout the rest of the thrust wedge. The increased strain rate shown in the figure is only present during the final stages of extension. In the first phase of extension, no variation in strain rate is visible. The final maximum height and width of the deformation zone are 44 mm and 15.3 cm respectively. No thinning of the layers in the unfaulted part of the model is visible.

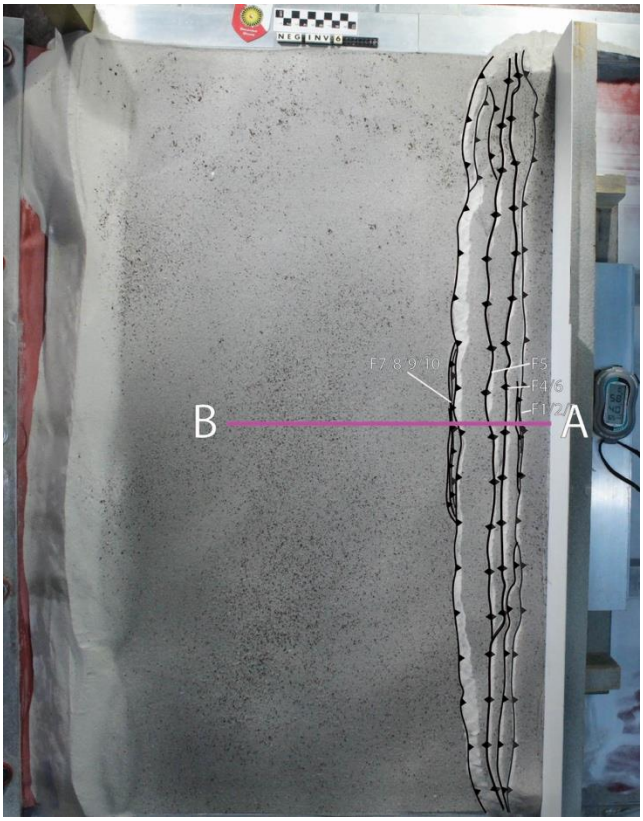

Figure 36: Top view image of NEG INV 6 after shortening completed.

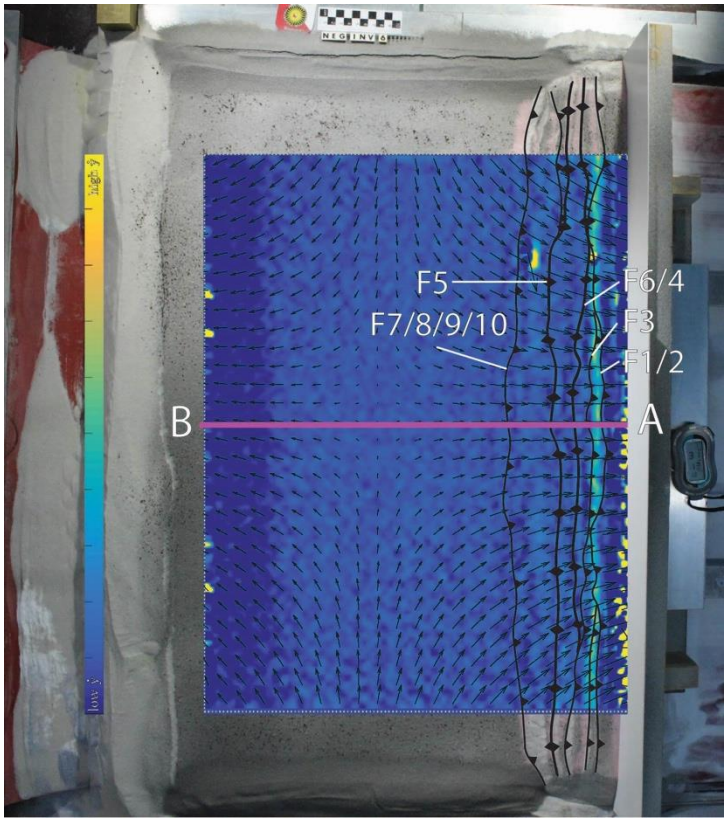

Figure 37: Relative strain rate variation during extension visualised over the top of NEG INV 6. It is visible that the highest strain rates are present at the location of the normal fault visible in the cross section. The location of the cross section through the model is shown.

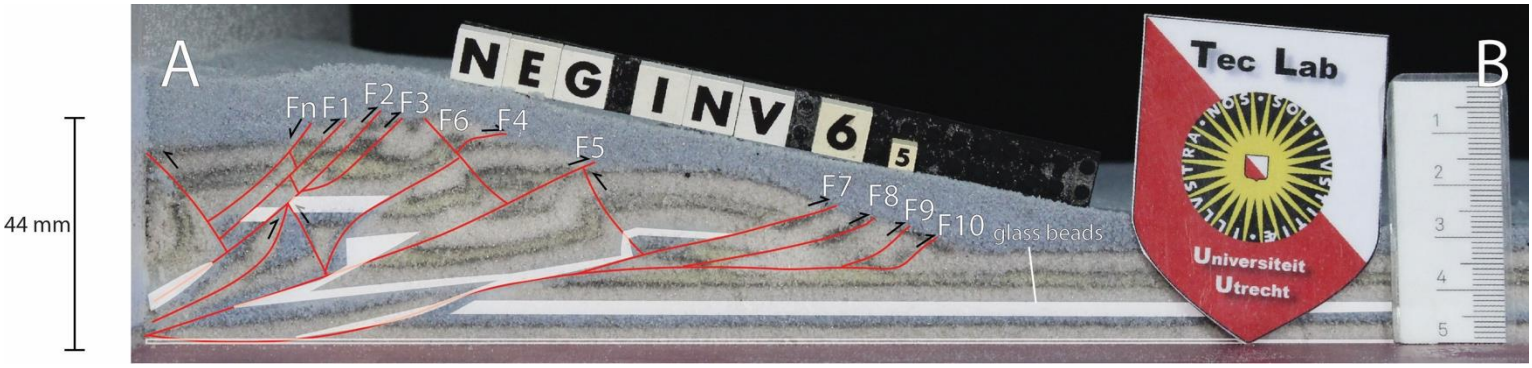

Figure 38: Cross sectional interpretation of NEG INV 6 along cross section 5.

3.3. Series iii

Series iii experiments are experiments that have a ductile decollement. The base 4 mm of all models are silicone putty (PDMS).

3.3.1. Compressional benchmark CBM1

Figure 39 shows the cross section of the compressional benchmark for series iii experiments.

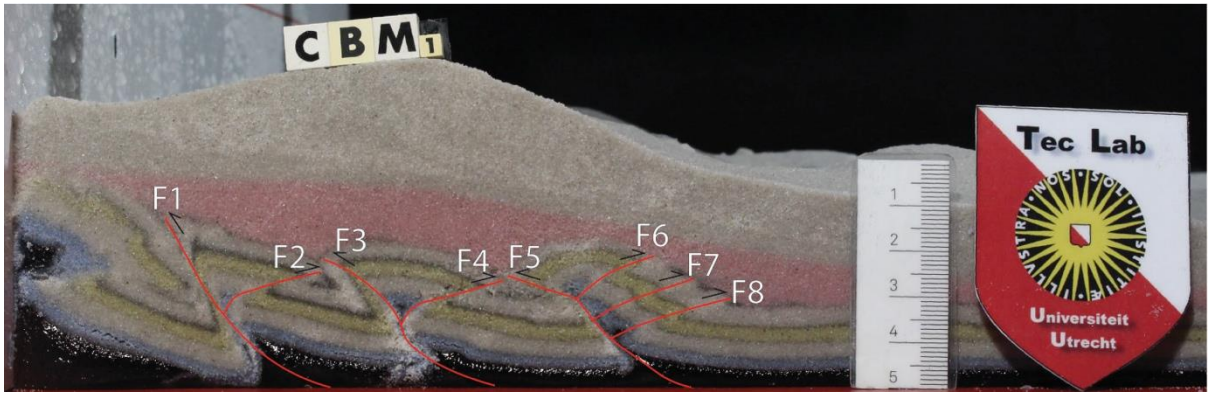

Figure 39: Compressional benchmark for series iii experiments.

The cross section shows that multiple pop-up structures develop in sequence from the backstop. The back thrusts that are part of these pop up structures are large, become increasingly lower angle faults as the fault propagated into the model. These back thrusts drag silicone putty up in to the model along their fault planes. The angles of the faults are shown in Table 6 below.

CBM1	angle [º]
F1	60
F2	16
F3	39
F4	16
F5	19
F6	23
F7	19
F8	16

Table 6: Fault angles of series iii compressional benchmark. Note the angles of F1, F3 and F5 are measured in their top parts close to the surface of the model.

3.3.2. NEG INV 7

This experiment makes use of a 4 mm thick base layer of silicone putty. During shortening the strength ratio is 3.2, during extension it is 1.1. The development of the thrust wedge is very sequential. The first faults develop close to the backstop, after which displacement occurs over these faults. Then new faults develop, further from the backstop and displacement occurs over these faults. The structures further from the backstop are pop-up structures. Figure 40 shows a top view image of NEG INV 7 after shortening completed. The width of the deformation zone after shortening is 19.2 cm.

These pop up structures are made up of multiple foreward thrust combined with a single backthrust. Backthrust F5 shows that silicone putty has been draged up along the fault plane.
When the deformation switches from shortening to extension, two normal faults develop. First, a normal fault (Fn1) develops close to the backstop. This fault cross cuts through the layers, as shown by the displaced markers. The second normal fault (Fn2) develops after Fn1. Fn2, which has an opposite dip direction compared to Fn1, starts by cross cutting layers but as is propagates deeper in to the model, it joins a weak backthrust that has silicone putty in it. This plane is reactivated during extension as the normal fault uses the weak plane to slide down. The final maximum thickness and width of the deformation zone are 32 mm and 23.3 cm respectively. No thinning of the layers in the unfaulted part of the model is visible.
Figure 41 shows the relative strain rate variations during extension of NEG INV 7. The image shows that the strain rate in the thrust wedge is noticeably higher than the unaffected areas. This indicates that the model is reactivating the thrust structures as it prefers to accommodate extension over these structures instead of creating new structures (faults). The strain rate variations also indicate that not only the weak plane of F5 is reactivated, but that all thrust planes are slightly reactivated even though this is not visible in the markers in the cross section. It is important to note that throughout the extensional phase strain rate variations are visible, but the strain rate variation is most apparent at the end of extension. Figure 41 is from the final stages of extension.

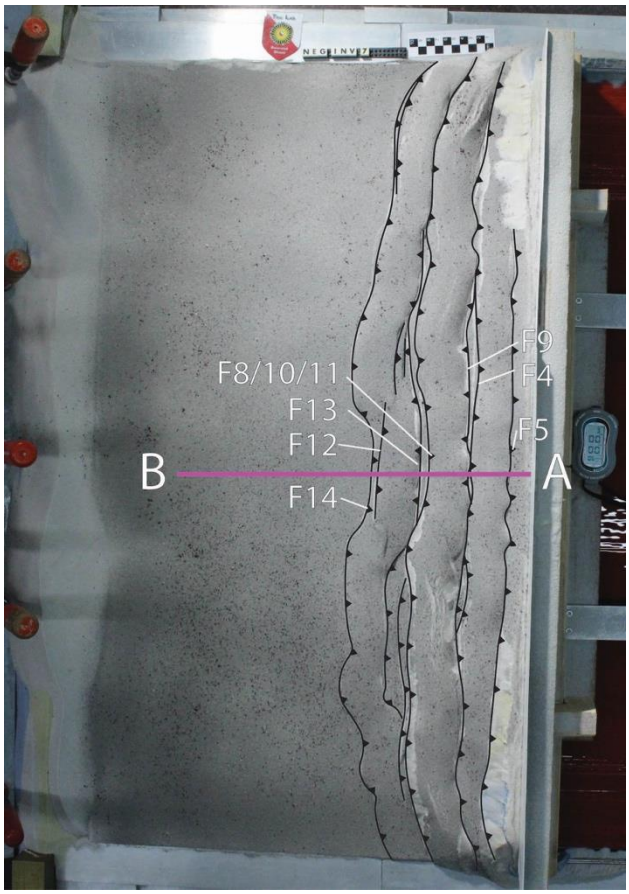

Figure 40: Top view image of NEG INV 7 after shortening finished.

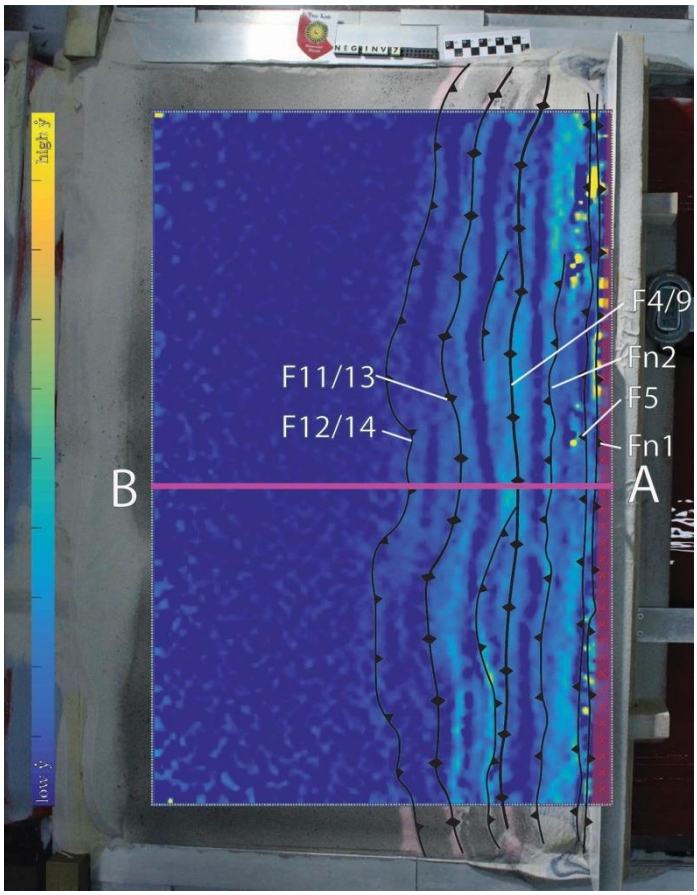

Figure 41: Relative strain rate variations during extension of NEG INV 7. The variation is based on the particle analysis. The image shows that there is a clear difference in strain rate between the thrust structures and the undeformed areas of the model. The location of the cross section is also visible in the figure.

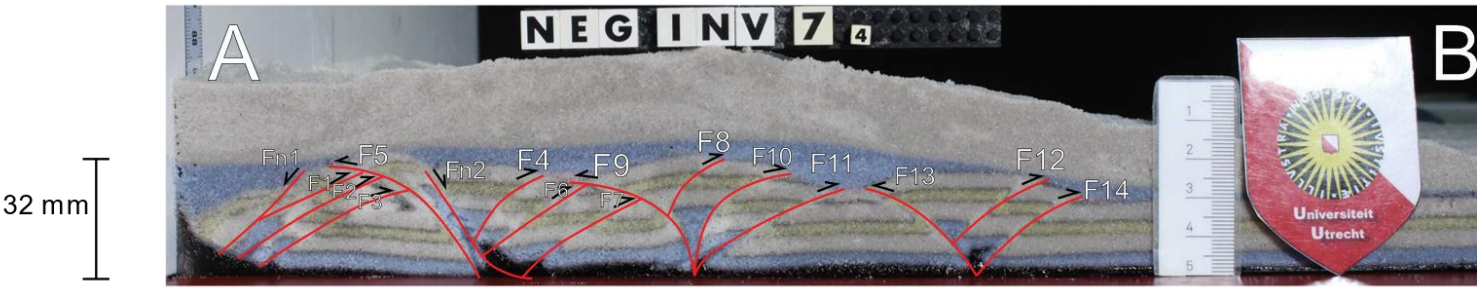

Figure 42: Cross sectional interpretation of the structures visible in cross section 4, NEG INV 7.

3.3.3. NEG INV 9

The goal of this experiment is to test the influence of a 5º tilt towards the hinterland on the reactivation of a thrust wedge in an extensional setting. The model is a brittle/ductile system with 4 mm putty at the base. During shortening the strength ratio is 3.2, during extension it is 1.1.

The model evolves by multiple forward thrusts close to the backstop that are later covered by a large back thrust. As shortening progresses, three more pop up structures develop. Each time a new pop up structure develops further away from the backstop. In total four pop up structures develop. Silicone putty is dragged up along the faults. After shortening, the width of the deformation zone is 17.4 cm. Figure 43 shows a top view image of NEG INV 9 after shortening completed.
During extension, 4 normal faults develop. Two large normal faults (Fn1 and Fn2) and two smaller normal faults (Fn3 and Fn4). Fn1 and Fn2 show very similar characteristics. At the surface of the model they start in a previously unfaulted area, but as they propagate deeper into the model, where the model is becomes increasingly stronger (Figure 20, page 22), they join on previously formed thrust planes that brought putty up. As they join on the thrusts, they angle of the normal faults becomes less and less. These planes are reactivated during extension.

Figure 44 shows the relative strain rate variations that occurred during final stages of extension of NEG INV 9. The figure shows that the structures that formed during shortening have relatively higher strain rates than the surrounding areas. This indicates that the structures are reactivated during extension. All structures seem to be reactivated at roughly the same strain rate, thus no specific plane is preferred. This confirms the interpretations made in the cross section and it provided further insight in showing that all structures are reactivated. Not only the structures in which the reactivation can clearly be seen in the cross section based on the markers. The reactivated faults that don't show normal displacement have had more reverse displacement during shortening than normal displacement during reactivation.

The final maximum height and width of the deformation zone are 33 mm and 22.1 cm respectively (a 5.2% decrease in deformation zone width with respect to the un-tilted experiment). No thinning of the brittle layers in the unfaulted parts of the model is visible. The silicone putty does show severe thinning (up to 100%) at some locations (beneath F5).

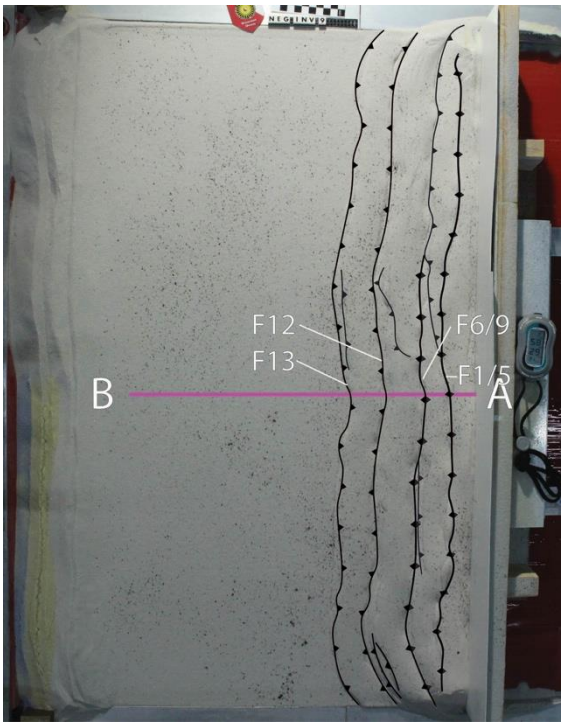

Figure 43: Top view image of NEG INV 9 after shortening completed.

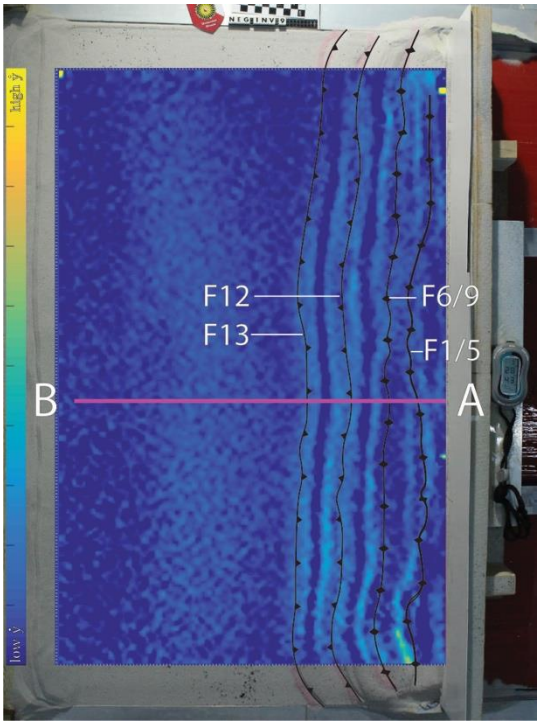

Figure 44: Relative strain rate variations during final stages of extension of NEG INV 9. It is visible that the thrust structures formed during shortening are being extended at relatively high strain rates compared to the rest of the model. This is indicative of reactivation occurring along the structures that formed during shortening. The location of the cross section is shown in the figure.

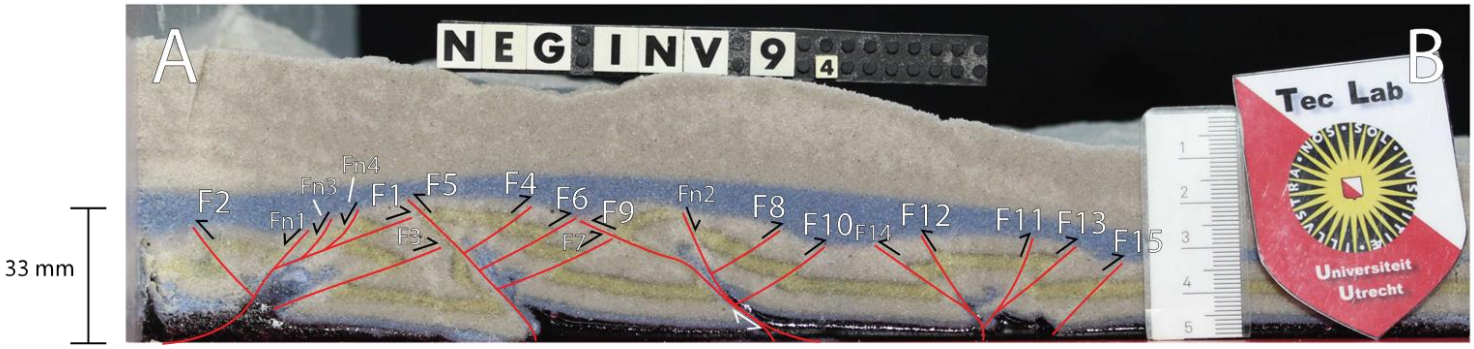

Figure 45: Cross sectional analysis of cross section 4 through NEG INV 9.

3.3.4. NEG INV 8

This experiment aims to investigate the influence of a much lower strain rate i.e. a larger strength difference; lower coupling. During shortening the strength ratio is 16.0, during extension it is 5.3. The model evolves by first forming a large thrust (F1?) and possibly simultaneously a thrust fault with a ramp/flat geometry. Later, as shortening progresses, two pop up structures develop. One defined by F3 and F4 as back- and forward thrust faults respectively, the other is made up of F5 and F6 as outer faults. Both pop up structures dragged silicone putty up in the model on their plane. Figure 46 shows a top view image of NEG INV 8 after shortening completed. The width of the deformation zone after shortening is 13.7 cm. When extension commences, it is accommodated in two ways:

i) A normal fault develops (Fn1) close to the backstop, dipping towards the backstop, that at the surface cross cuts layers and at depth joins the ramp portion of a thrust fault, reactivating it.
ii) A normal fault develops (Fn2), dipping away from the backstop, that again at the surface cross cuts the layers and deeper in the model the fault join the fault plane of F3 that contains silicone putty. This fault plane is significantly reactivated as nearly the entire pop up structure has slid down the plane containing silicone putty.

Figure 47 shows the relative strain rate differences that occurred during final stages of extension of NEG INV 8. The image shows that at the location of the two normal faults discussed above, the strain rate is highest. It is also visible that at the location of the pop up structure furthest away from the backstop, the strain rate is slightly elevated. This indicated that that structure is also reactivated, even though it is not visible in the markers. The image also shows that there is a diagonal component in that shows elevated strain rate. This component has not occurred in any other experiment. It is important to note that, after terminating of this experiment, significant amounts of silicone putty had extruded and was exposed. The locations of the diagonal strain rate elevation and the exposed silicone putty are both roughly in the same spot and are possibly related.

The final maximum thickness and width of the model are 34 mm and 18.9 cm respectively. No thinning of the brittle layers in the unfaulted parts of the model is visible. The ductile layer does show strong thinning at some locations (beneath F3).

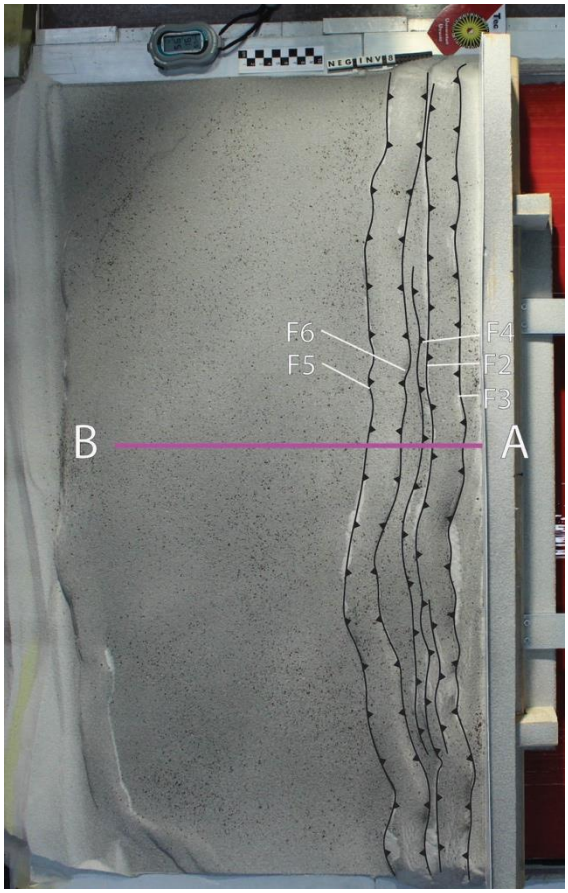

Figure 46: Top view image of NEG INV 8 after shortening was completed.

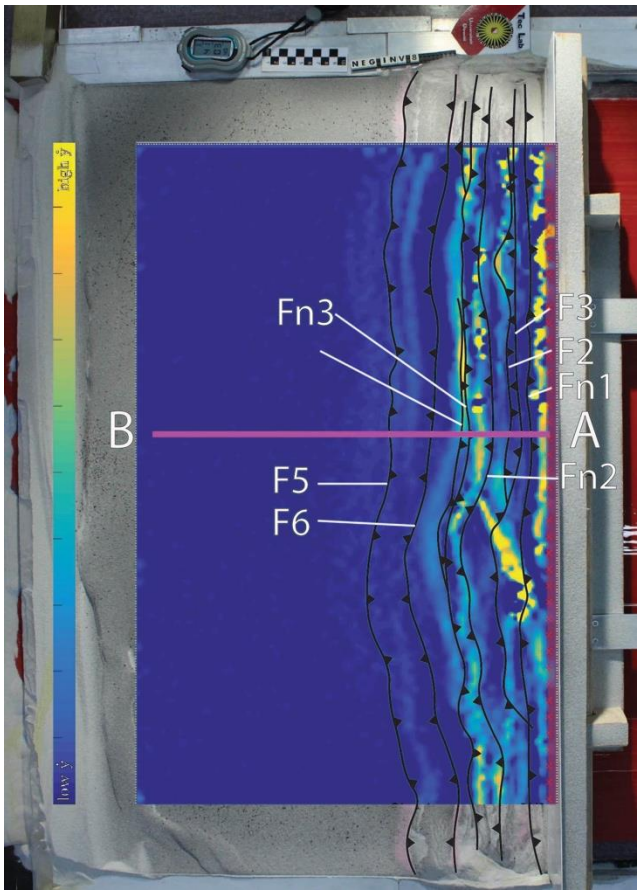

Figure 47: Relative strain rate variations that occurred during extension of NEG INV 8. The image shows that at the location of Fn1 and Fn2 in the cross section the strain rate is highest. At the location of the pop up structure made up by F5 and F6 a slight elevation in strain rate is visible. The image shows a discrepancy with respect to strain rate variation from other experiments as a diagonal component is visible. The location of the cross section is shown in the figure.

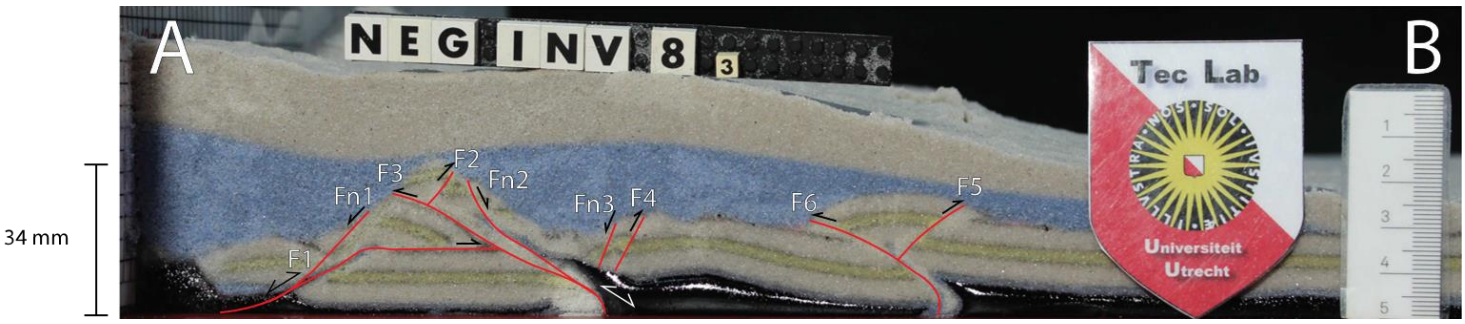

Figure 48: Cross sectional interpretation of cross section 3 through NEG INV 8.

3.4. Summary of modelling results

In the following paragraph, key modelling results are summarised and some comparisons will be made between the experimental series.

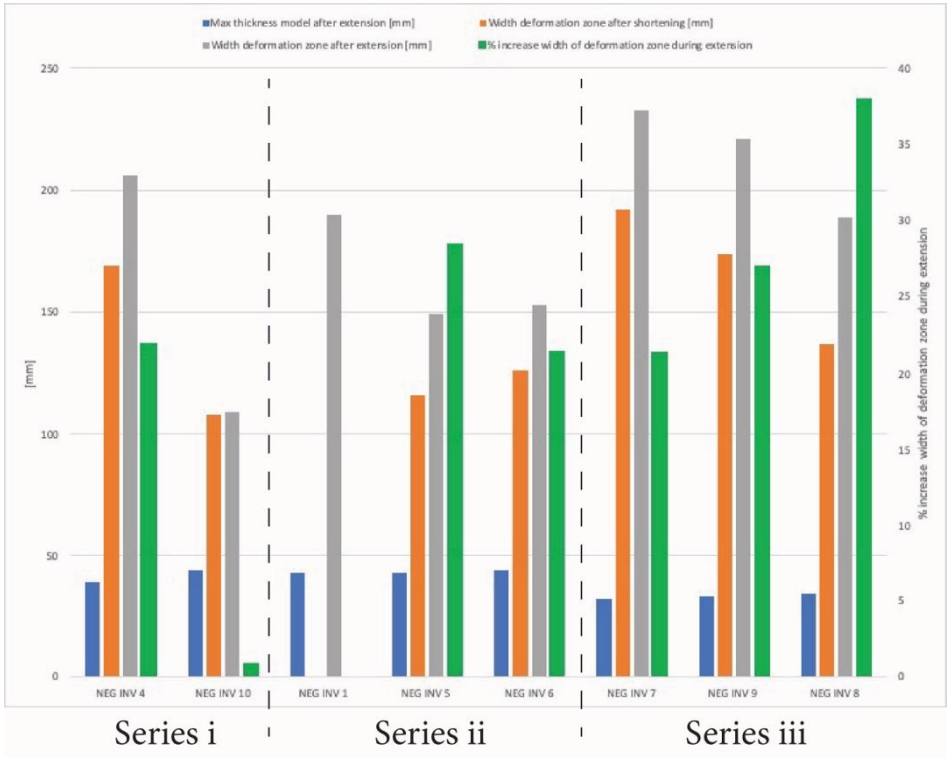

Figure 49: Overview of the final height and width of the deformation zones of all discussed experiments. Note that for all experiments that have a 5º tilt, the width is always shorter than their tilt-less counterparts. Whilst the thickness increases or remains the same with tilt. The experiments that have tilt are NEG INV 10, 5 and 9.

		Max thickness model after extension [mm]	Width deformation zone after shortening [mm]	Width deformation zone after extension [mm]	% increase width of deformation zone during extension
series i	NEG INV 4	39	169	206	21,9
	NEG INV 10	44	108	109	0,9
series ii	NEG INV 1	43	N/A	190	N/A
	NEG INV 5	43	116	149	28,4
	NEG INV 6	44	126	153	21,4
series iii	NEG INV 7	32	192	233	21,4
	NEG INV 9	33	174	221	27,0
	NEG INV 8	34	137	189	38,0

Table 7: Data on the thickness of the models, the widths of the deformation zone after shortening and after extension and the amount of elongation of the wedge per model.

Figure 49 present a bar chart of all final thicknesses and widths of deformation zones both after shortening and after extension. Table 7 shows the data that supports the bar chart. A trend is visible where the tilted experiments have a shorter deformation zone than their un-tilted counterparts after the experiments are completed. For the brittle experiments this is a very large difference (47% decrease) whilst the low friction models show a 22% decrease and the brittle ductile model shows a 5% decrease. The percentage increase of the width of the wedge between shortening and extension is also given (i.e. the elongation of the wedge during extension). It is

remarkable that a tilted brittle only model will barely be elongated (0.9%) whilst the flat brittle model follows the same trend as the other experiments (20-30% elongation during extension). The final thickness of the model increases (or in the case of the tilted low friction glass beads model) remains the same with tilt.

Regarding the thinning that was observed in the models, no trend can be distinguished. Only two models showed thinning. NEG INV 4 (un tilted, brittle only) shows 10% thinning. NEG INV 5 (tilted, low friction with glass beads at base) shows 5% thinning. These models have no clear parameter trends either as the models are both tilted and untiled and have distinct base frictions.

As mentioned before, Figure 50 is a collection of all presented cross sectional analyses in this thesis. All cross sections have the same scale and the edge (left sides) of all deformation zones are aligned by the dotted red line. The main characteristics are the shorter widths of the tilted experiments and the reactivated thrust planes that are mainly visible in series iii experiments. Series ii NEG INV 5 (tilted, low friction glass beads base) also shows a partly reactivated thrust fault.
Figure 51 is an overview of all relative strain rate variations that are presented in this thesis. These figures indicate that the models that contain silicone putty have thrust structures that are being reactivated in extension. The colour difference that can be seen (light vs. dark blue) in combination with the structure being drawn on the image show that the thrust structures deform faster than the surrounding areas. The models with glass beads as a base layer also show slightly elevated strain rates along the thrust structures, indicating that they are partly reactivated.

Series i experiments show that during the un tilted brittle experiment, no normal faults develop but a 10% thinning of the layers is deduced. This is different from the tilted brittle experiment, that shows a clear normal fault cross cutting the layers. This behaviour is consistent with the work of Krantz (1991). During this experiment no thinning is observed. The strain rate variation analysis indicates that the wedge is not deforming faster than the rest of the model. However, this does not mean that the wedge is not being extended over the thrust plane of F6. Combined, Fn and F6 accommodate the extension applied to the model. This series shows that introducing tilt to the system leads to the development of shorter thrust wedges during shortening and also leads to the normal faults during extension. During the un-tilted experiment, NEG INV 4, extension must be accommodated by other means. In this case it is accommodated by thinning of the layers. The strain rate analyses of this series (Figure 24 and Figure 27) indicate that the thrust structures are reactivated in the un-tilted model that did not have any normal faults (NEG INV 4). Important to note is that this reactivation is only visible during the first phase of extension as during the first stages of extension the angels of the thrust faults are still favourable for reactivation to occur (>40º, Krantz, 1991). As the faults are rotated counterclockwise during extension, the angles become lower and the faults are no longer reactivated. After roughly 20% extension has occurred, the strain rate variations (and thus the reactivation) disappear. From this point on deformation occurs evenly over the model.

Series ii models show severe thinning. In NEG INV 1 (un tilted) and 5 (tilted) the blue and yellow layers are severely thinned, in NEG INV 6 (extra layers of glass beads) the extra glass beads layer is severely thinned. In an attempt to confirm this is caused by extension, a compression only benchmark experiment is run with glass beads in the centre of the model. However, this experiment also shows severe thinning of the glass beads layer. This indicates that the thinning is caused during shortening and that perhaps the thinned layers are used as glide planes. This observation shows that during shortening of series ii experiments stratigraphic contacts are used to accommodate shortening. This indicates that only layers that are in contact of close to the structure are thinned. The compressional benchmark that only has glass beads at the base of the model do not show the same thinning of quartz layers. Thus the thinning of the blue and yellow layers during the un tilted model is a result of extension.

During series ii experiments no thrust structures are significantly reactivated during extension, only new normal faults developed during NEG INV 5 (tilted) and NEG INV 6 (extra layer of glass beads) close to the backstop. The lack of reactivation observation is also backed in the relative strain rate variation figures (Figure 31, Figure 34 and Figure 37). These figures indicate that relatively high strain rates are only visible in the location where normal faults develop close to the backstop. This series of experiments follow the trend that introducing tilt to the system localizes deformation both during shortening and extension the final width of the deformation zone is shorter in the tilted experiment during both phases of deformation.

All series iii experiments consistently highlight the following key points. During shortening of series iii models, silicone putty is dragged up higher in the model along thrust ramps. Often this occurs via a large back thrust but can also happen at a forward thrust and beneath pop up structures. When the deformation switches from shortening to extension, normal faults develop above these (back) thrusts containing silicone putty. At the surface of the model, these normal faults develop in unfaulted areas. As they propagate deeper in to the model, where the model becomes stronger, these normal faults change their angle and join on the weak planes that contain silicone putty. The compressional benchmarks prove that the upward propagation of the silicone is a result of shortening and not of extension. Once the faults join these planes, the planes are reactivated and accommodate extension. This is visible in the cross sections (Figure 42, Figure 45 and Figure 48) by observing the offset along the faults. It is also visible by studying the relative strain rate variations (Figure 41, Figure 44 and Figure 47) as these clearly show that the extension is accommodated by reactivation of part of the thrust structures that brought some silicone putty up in the model. The strain rate variations figures show this by heightened strain rates above the locations where the normal faults join the pre-existing thrust planes. Such clear reactivation is not observed in series i and ii. This proves that in order for reactivation to occur, a weak zone/plane is required (strength profiles: Figure 19, Figure 20 and Figure 21) . Otherwise creating a new fault plane will always require less energy. This is a results of the difference between the angle of thrusting and the angle of normal faulting. The influence of introducing tilt to the system can be seen by comparing NEG INV 7 and NEG INV 9. As described above, the characteristics are similar in both the cross sectional analyses and the relative strain rate variation analyses. A difference that can be noticed is the localization of deformation that occurs during shortening after introducing tilt to the system.

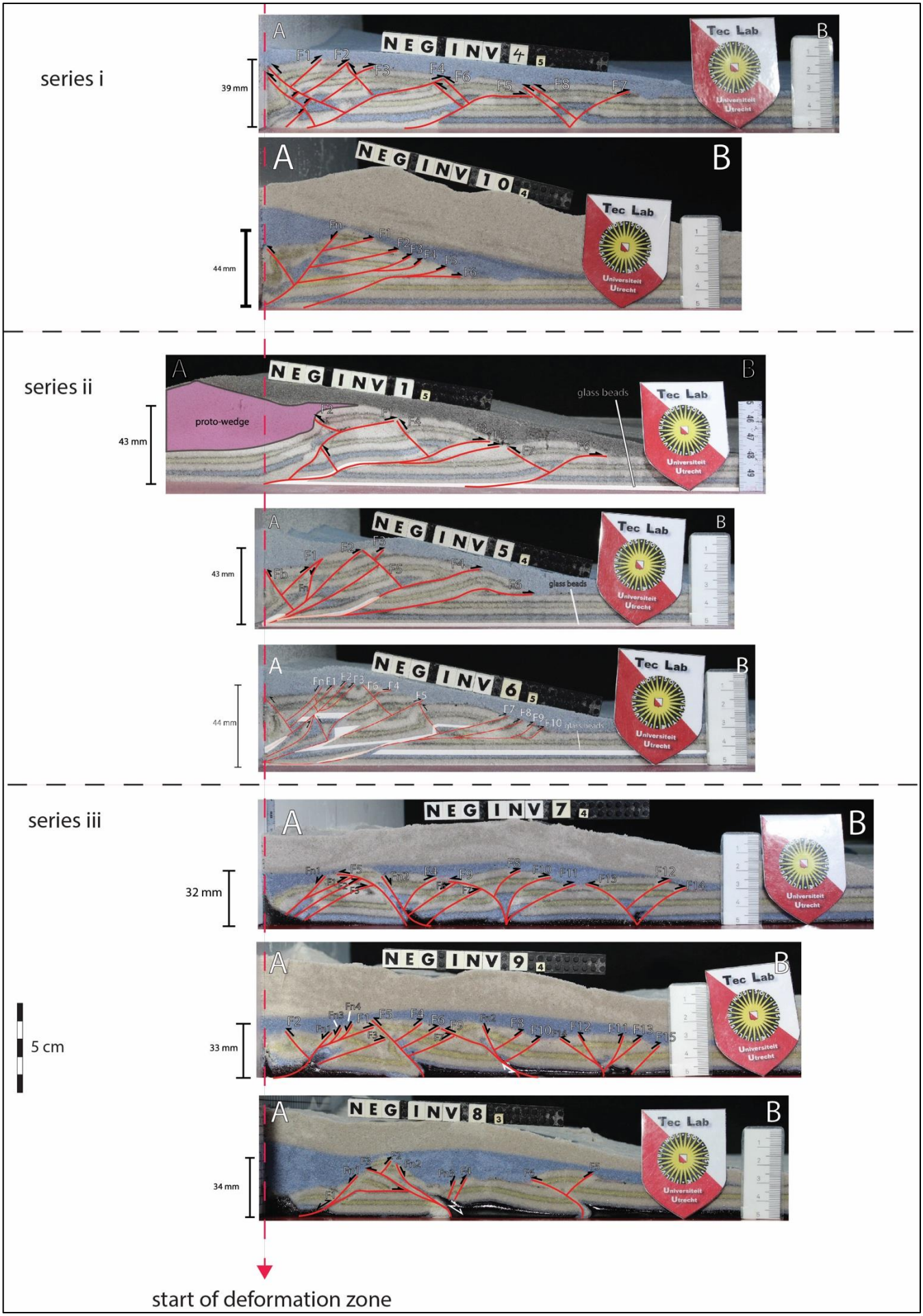

Figure 50: Overview of all interpreted cross sections presented earlier in this thesis. This figure is given as a convenience for easier comparison of results. Please refer back to each indivindual figure for remarks on the interpretations.

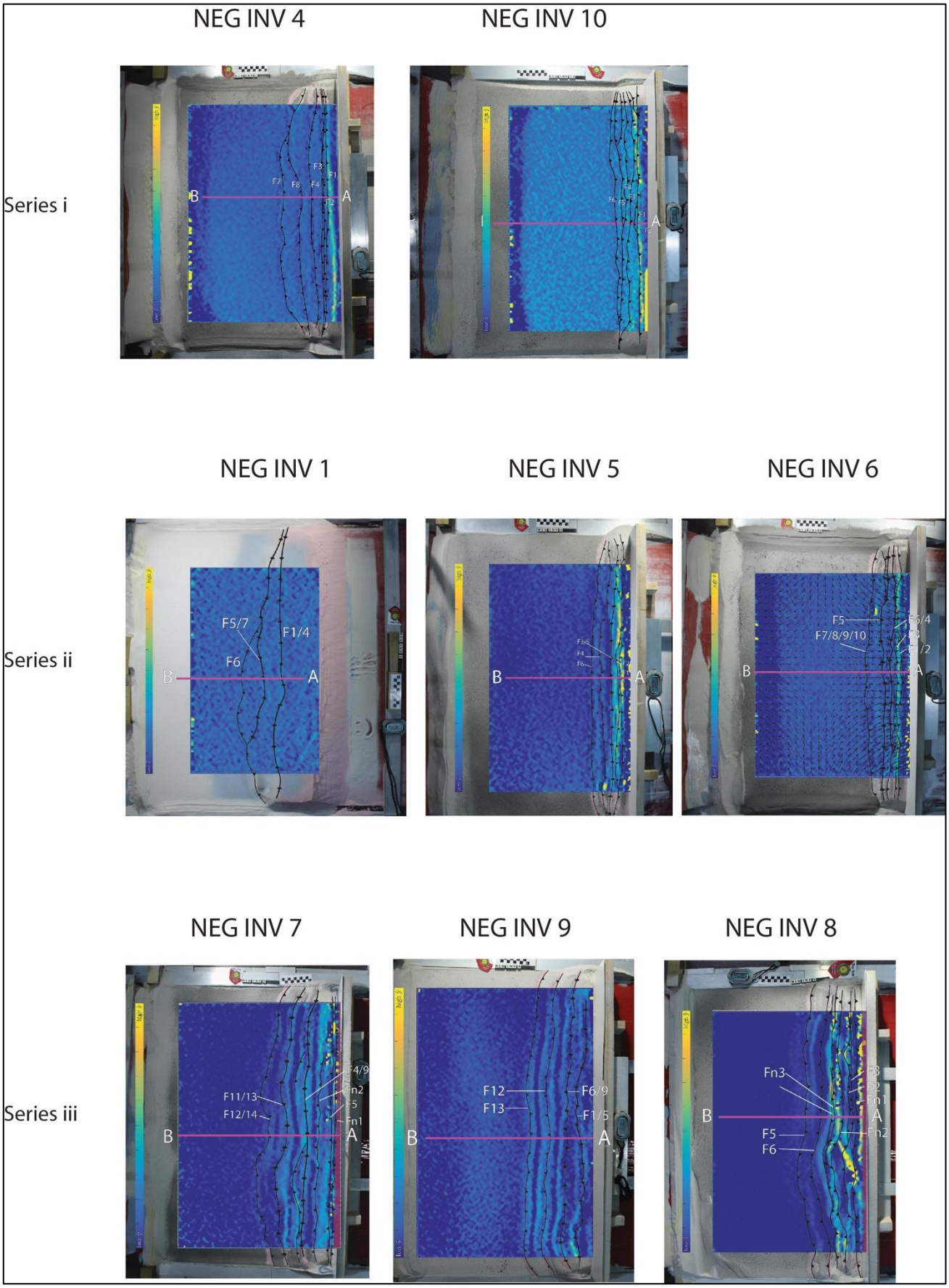

Figure 51: Overview of all relative strain rate variation figures presented earlier in this thesis. This figure acts as a convenient way to compare results.

CBM2	forward thrust angle [º]	back thrust angle [º]
F1	68	x
F2	x	45
F3	x	51
F4	x	53
F5	14	x
F6	x	66
F7	58	x
F8	22	x
F9	38	x
F10	24	x
Average:	37	54

NEG INV 4	forward thrust angle [º]	back thrust angle [º]
F1	42	x
F2	38	x
F3	27	x
F4	15	x
F5	29	x
F6	x	45
F7	27	x
F8	36	x
Average:	31	45

Series i

CBM3	forward thrust angle [º]	back thrust angle [º]
F1	x	46
F2	22	x
F3	21	x
Average:	22	46

NEG INV 1	forward thrust angle [º]	back thrust angle [º]
F1	21	x
F2	x	31
F3	19	x
F4	x	51
F5	13	x
F6	30	x
F7	x	32
Average:	21	38

Series ii

CBM1	forward thrust angle [º]	back thrust angle [º]
F1	x	60
F2	16	x
F3	x	39
F4	16	x
F5	x	19
F6	23	x
F7	19	x
F8	16	x
Average:	18	39

NEG INV 7	forward thrust angle [º]	back thrust angle [º]
F1	24	x
F2	27	x
F3	27	x
F4	38	x
F5	x	38
F6	32	x
F7	30	x
F8	42	x
F9	x	34
F10	35	x
F11	24	x
F12	30	x
F13	x	37
F14	39	x
Average:	32	36

Series iii

Figure 52: Angle data on all of the thrust faults of the compressional benchmark models and the thrust faults of their negatively inverted counterparts.

The thrust fault angles of all compressional benchmarks and their negatively inverted counterparts are shown in Figure 52. These tables show the angles of all forward and back thrusts and the average of each type. With the exception of forward thrusts in brittle ductile regimes, all thrusts are rotated to be less steep after extension. The forward thrusts in negatively inverted brittle/ductile regimes become steeper after extension (18º average to 32º average).

4. DISCUSSION

4.1. Looking back at the state-of-the-art

At the beginning of this thesis a section is presented in which all previously performed analogue experiments that are relevant for this research are discusses (section 1.4 State-of-the-art). Although limited amounts of research has been done, each research group produced some comparable data. In this section the findings of this thesis will be compared to the results presented in the other research papers, namely those by Faccenna et al. (1995) and Krantz (1991).

Faccenna et al. (1995) showed that pre-existing thrust faults had to have angles of 41º ± 1º in order for extensional reactivation to occur. This result is also produced in this thesis e.g. NEG INV 10, Figure 28, page 28, where the thrust faults are not reactivated. Instead, a normal fault develops that cuts all thrust faults. The paper also described that normal faults branch from thrust faults at the décollement level if the thrust was dipping 32º ± 1º. This thesis does not constrain the dip angle correlation but similar behaviour is visible in terms of a normal fault developing that later join in on the plane of a thrust fault at decollement level (e.g. NEG INV 5, NEG INV 7, NEG INV 9 and NEG INV 8).
The experiment performed by Krantz (1991) that used a rubber base shows somewhat comparable results to this thesis. The paper shows that thrust faults rotate to ~60º during extension as a result of counter clockwise rotation. This is also visible in NEG INV 8 (Figure 48) in F2 and F4. However, it is important to note that Krantz (1991) only used quartz sand and that NEG INV 8 makes use of both brittle and ductile materials. This indicates that the rotational behaviour occurs in both rheologically homogeneous and heterogenous areas. This is different from the results of this thesis where we only see the steepening of faults for brittle/ductile systems. Our results are based on multiple experiments with averaged angles, whilst the Krantz (1991) only ran a single experiment with a rubber base.

4.2. Influences of tilting the system

All experiments show that increasing the tilt of the system causing deformation to localize both during shortening and during extension. This is a result of the base friction increasing after tilting, as the normal component of the base increases when pushing up a slope, and deformation localizing with increasing base friction. Base friction in a model translates to basal coupling in nature where the different frictional values would be governed by rheological differences. A higher basal coupling increases the tapered wedge and vice versa (Davis, 1983). The localization of deformation is present during both shortening and extension. The widths of the deformation zones after shortening and after extension are always shorter for the tilted experiments. As a result of the localized deformation occurring in a tilted system, the maximum thickness of the models increases. Tilting the system also increases the likelihood of a thrust fault being reactivated. This can be seen in the tilted low friction model that has glass beads at the base (NEG INV 5). This series shows that a thrust wedge that is tilted has thrust faults that are rotated as a result of extension (increasing angle) and have increased angles due to the tilt affecting the system. This allows for the thrust faults to be reactivated in extension, in accordance with (Krantz, 1991).

4.3. Influences of frictional versus ductile decollements

As described in section 3.4 Summary of modelling results, models that contain silicone putty as a basal decollement drag this silicone putty up in the model during shortening. The series iii

compressional benchmark experiment proves that this upward migration of weak silicone is occurring as a result of shortening. When such systems develop a thrust wedge, multiple forward and back thrusts develop. These thrust drag silicone putty up along these contacts. The thickness of the dragged silicone putty decreases as it is dragged higher in the model. The moment such thrust wedges are negatively inverted, new normal faults always develop above such thrusts that contain silicone putty. These new normal faults propagate down in the model and join on the weak planes of the silicone putty bearing (forward/back) thrusts. The faults favour this opposed to faulting new areas as the weakness of the silicone putty compared to the strength of the quartz compensates for the difference in optimal faulting angle. The angle of the normal fault decreases as they follow the geometry of the silicone putty. Such a change in angle is also documented by Krantz (1991).
The influences of tilting the system and the influence of having a multi-rheological system are visualised in Figure 53 below.
This shift in extensional behaviour between frictional and ductile decollements produces another distinct characteristic of the cross sections. Figure 52 shows all thrust fault angles of the compressional benchmarks and their negatively inverted counterparts. These results show that the reactivation of a system with a ductile decollement causes the forward thrusts to be rotated and become steeper. This can be linked to the extension behaviour as the significant reactivation of back thrusts in ductile domains rotates the forward thrust to greater angles as large blocks rotate whilst sliding down these reactivated contacts. Whilst the frictional extension in brittle system causes the forward thrusts to become less steep. This is a result of extension not being significantly accommodated by large contacts, which would rotate the faults. Instead, all areas (and thus faults) are stretched from both sides, sliding in both directions, flattening the faults.

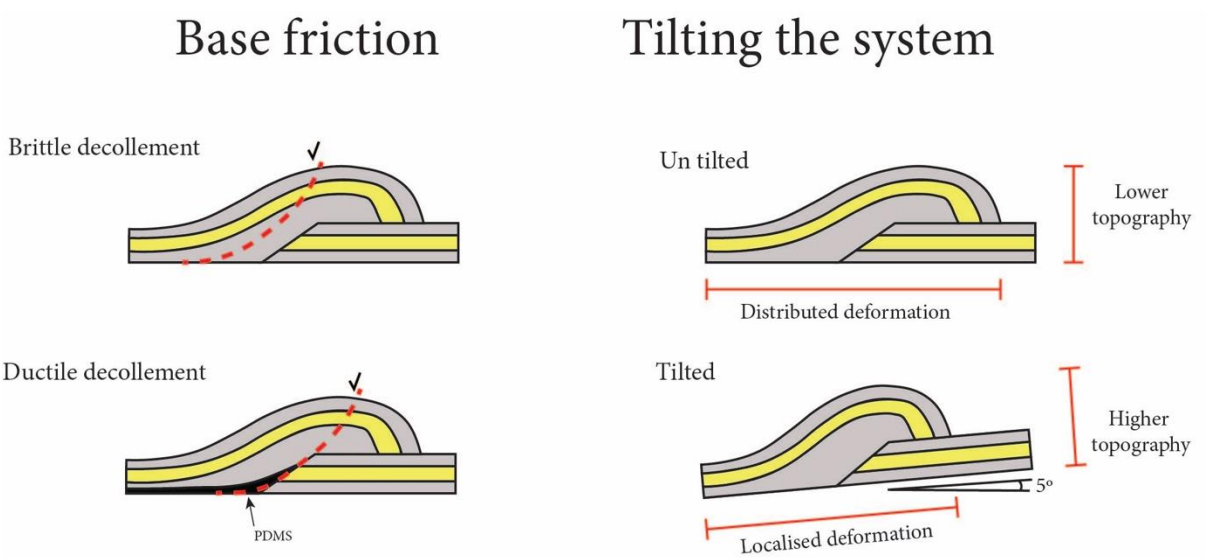

Figure 53: Visualisation of the main results presented by the experiments. On the left the influence of distinct basal frictions is shown. In these illustrations, the location of geometry of a future normal fault is given, if the system were to be negatively inverted. On the right the influences of tilting the system (5º towards the hinterland) are shown. The changes is deformation localization and topography are accentuated.

An interesting results comparison can be made between the high and low strain rate un-tilted experiments (NEG INV 7 and NEG INV 8 respectively). The strength profiles of these experiment are different in the way that the strength ratios are very different. Namely for NEG INV 7 during

shortening = 3.2, during extension = 1.1 and for NEG INV 8 during shortening = 16.0, during extension = 5.3. Furthermore, the results are similar in that both experiments produce a back thrust that drags silicone putty higher up in the model. Later, during extension, this area is reactivated. These two experiments also showcase phenomena where deformation is distributed during both shortening and extension with increased strain rate, which can be seen in the widths of the deformation zones. Such a process was also described by Brun et al. (2016) as they show that extension distributed in the Aegean after slab rollback acceleration occurred. This indicates that the localization of deformation is strongly related to the amount of coupling in a system. As Brun (2002) describes that lower strain rates result in the lower crust acting as a décollement layer as a response to lower coupling between the upper and lower crust.

For all experimental series, the observable amount of extension in the cross sections and by studying the relative strain rate variations seems to be incoherent with the amount of extension applied to the systems (12 cm per side, 24 cm in total). It is true that this 12 cm extension per side does not translate 100% to 24 cm extension in total as the rubber sheet is acting as a buffer and accommodating some of the extension beyond the boundaries of the models. During the testing phases of the set up actual extension turned out to be ~16 cm in total after applying 24 cm in total. The amount of extension during the actual experiments is also considered to be ~16 cm, although this cannot be measured in the same way as during the testing phase due to the model obstructing the view of the rubber sheet.

During series iii experiments, extension is occurring throughout the model at locations that are not per se associated with the main tectonic contacts. This could be in the form of unobservable (due to lack of markers) stretching and shearing happening within the ductile layer. A similar process is described by e.g. Porkoláb et al. (2019) and Vissers et al. (1995). They describe ductile exhumation being accommodated by shear zones and shearing that are located between the main shear structures. When converting this back to the series iii experiments presented in this thesis, such shearing occurred during severe thinning of the ductile layers.

4.4. Relevance of modelling results for natural examples

Ustaszewski et al. (2010) show that the Cenozoic Adria-Europe plate boundary comprises of the Sava zone. This zone underwent Late Cretaceous subduction that resulted in the formation of a suture zone. Ultimately, an accretionary wedge developed as a result of continent-continent collision. During the Miocene a low-angle detachment develops that is cut by high-angle normal faults during later stages of extension (Ustaszewski et al., 2010)

This detachment contains sericites, based on which the age is partly constrained, that could act as a weak layer. The relative weakness is a result of the very fine grained mica's of which it consist. To further clarify their findings, they present a crustal scale geological cross section of the Sava Zone (Figure 54). The figure shows that the large detachment fault is cross cut by smaller normal faults, which thus must have developed later than the detachment fault.

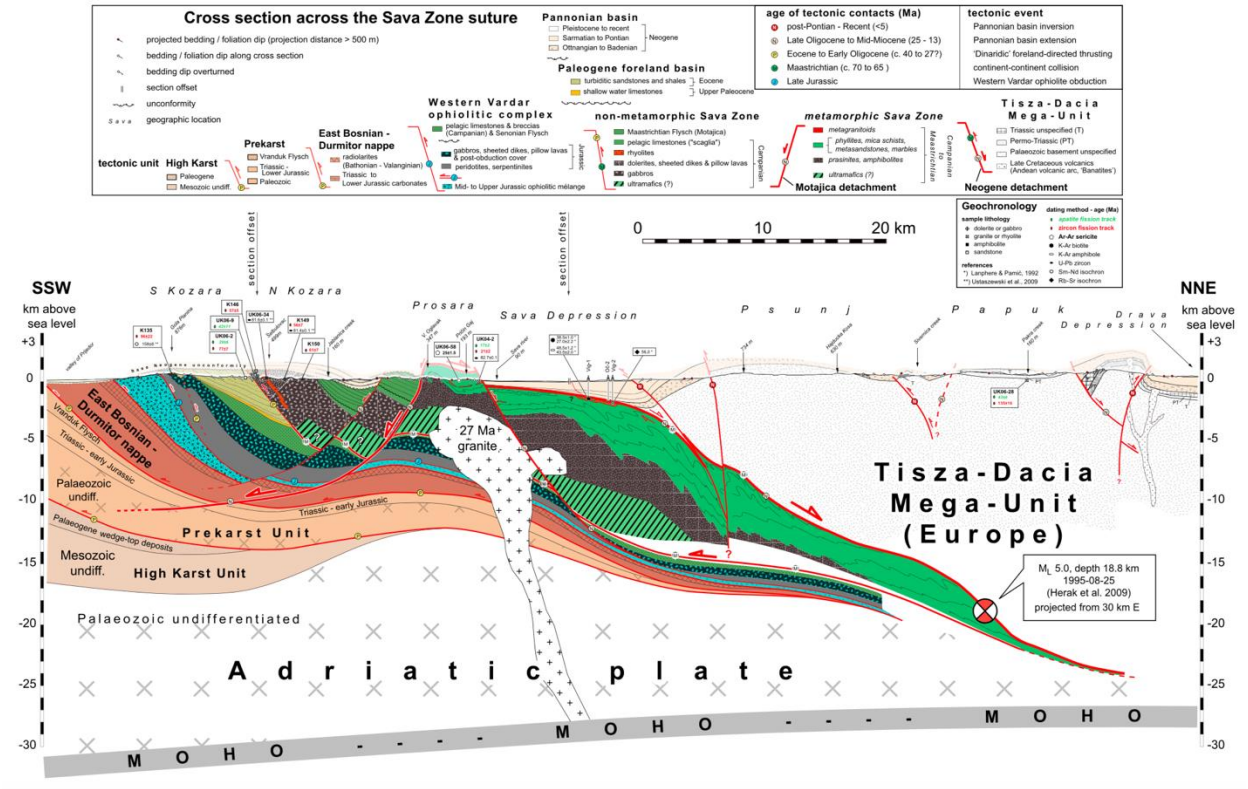

Figure 54: Crustal-scale geological cross section of the Sava Zone. Modified after Ustaszewski et al. (2010).

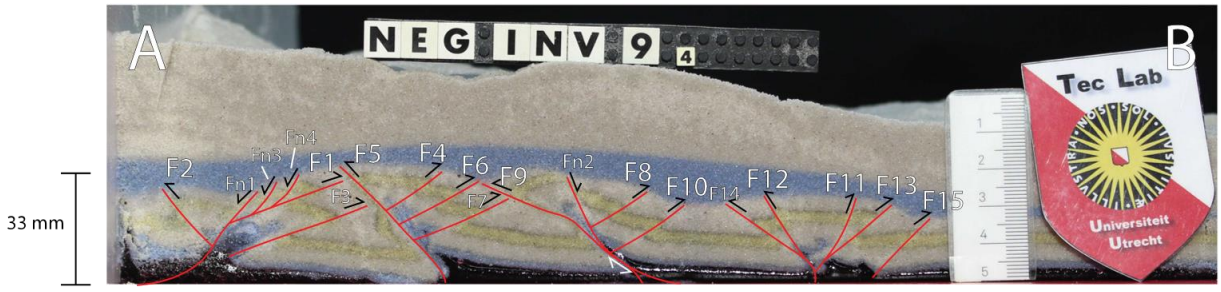

Figure 55: Cross sectional analysis of cross section 4 through NEG INV 9.

When comparing the structures in Figure 54 to the structures that series iii experiments developed, some comparisons can be made. Especially NEG INV 9 (Figure 55) shows the combination of a detachment fault related to a weaker area (Fn2) and some smaller, high angle normal faults (Fn1, Fn3 and Fn4). However, the interplay between these features is different during NEG INV 9 than in the Sava zone as during NEG INV 9 the high angle normal faults do not interact with the detachment fault. Instead, they develop independently from each other. However, there is a feature that NEG INV 9 does share with the Sava zone and that is that there is an area that remains unaltered after the onset of extension. In the Sava zone (Figure 54) this is the Prosara area that partly comprises of a granitic intrusion, in the model (Figure 55) this is the area between Fn4 and Fn2. Both areas are confined by normal faults that dip in opposite directions, leaving the area in between the faults as elevated terrain compared to the surrounding terrains.

These similarities confirm the validity of the experimental set up and indicate that a tilted (5º) basement is the configuration that yields the most true results when comparing to nature. Consequently, the results produced during the experiments provide valuable insight as to how

thrust structures behave when subjected to (uniform) extension. Particularly the requirement for rheological variations (i.e. weak shear zones or weak faults) for reactivational behaviour (as only series iii experiments show significant reactivation) is supported by this study.

Another research on negative inversion in the Dinarides is published by van Unen et al. (2019). They show that slab detachment during the Oligocene lead to Miocene extension throughout the entire Dinarides. In this research paper, they provide two geological cross sections (Figure 56) showing that thrust faults are reactivated as normal faults. The normal fault at "Durmitor Flysch"

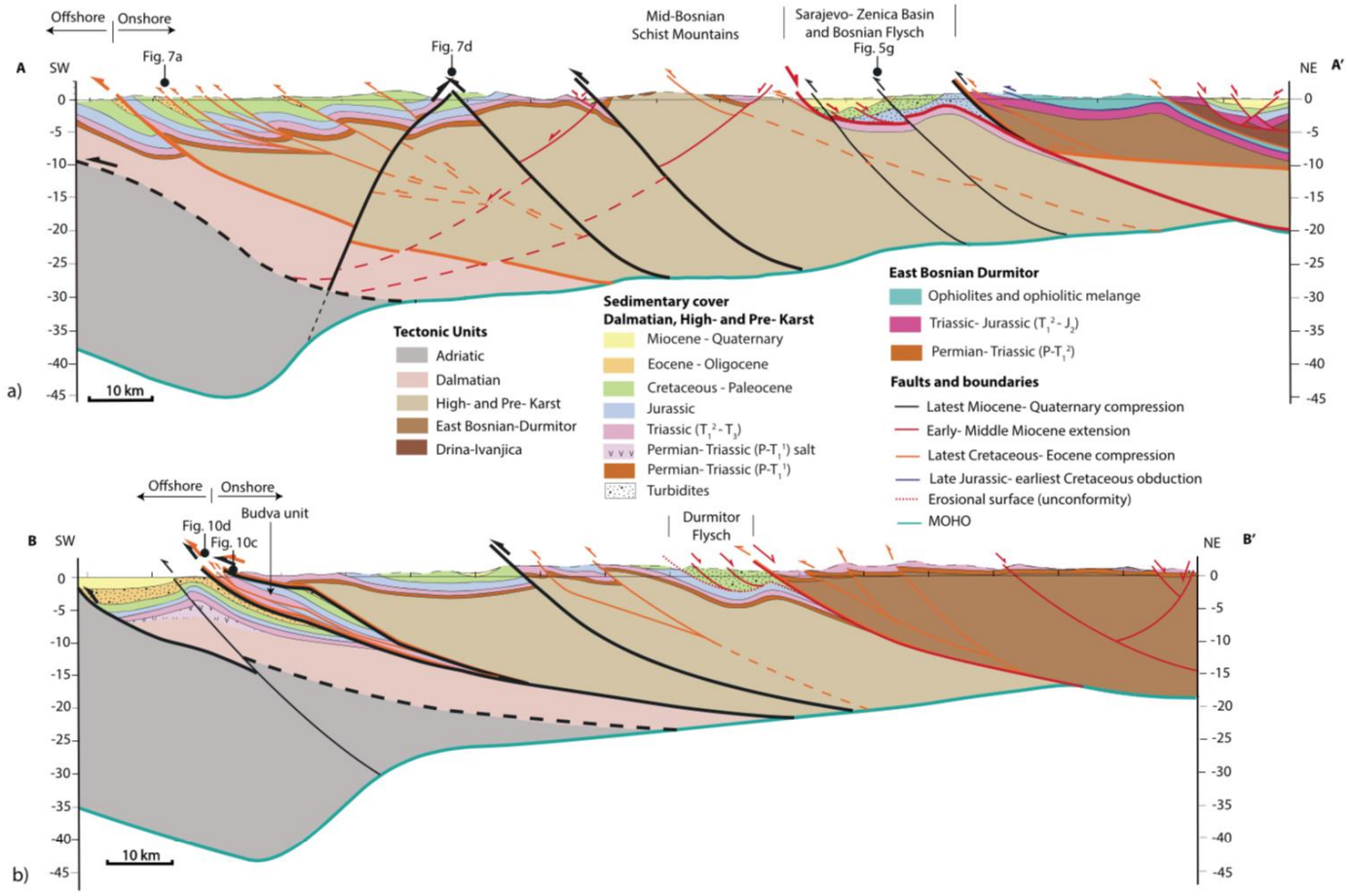

Figure 56: Geologic cross section through the Dinarides. Modified after van Unen et al. (2019).

in cross section b of Figure 56 show such a reactivated thrust fault. The cross section shows that reactivation only occurred over the large scale thrust fault. This is also visible in the cross section of NEG INV 9 shown above (Figure 55) where albeit the geometry is different, reactivation is only occuring on the large thrust fault. The large thrust fault shown in (Figure 55b) shows that the fault crosses 10 km depth, the same thickness as NEG INV 9. It is reasonable to believe that this thrust fault dragged some weaker material up into the crust, that enabled it to later be favourable for reactivation. As can be seen in Series iii experiments where only thrust faults that dragged silicone putty up in the model are reactivated.

Another interesting research to compare these results to is the research published by D'Agostino et al. (1998). They discuss the role of pre-existing thrust structures on the style of extension in the Apennines. They describe that the lower low-angle thrust is extensionally reactivated. This in turn causes antithetic faults to develop, rotating the hanging wall of the system (Figure 57).

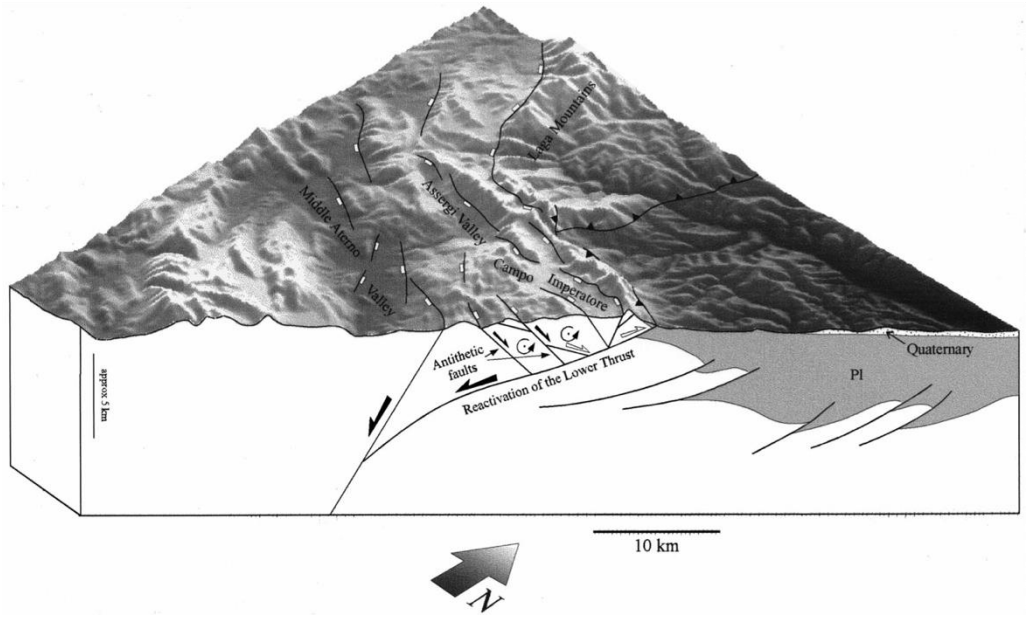

Figure 57: Schematic cross sectional analysis of the Campo Imperatore plain with incorporated antithetic faults. Modified after D'Agostino et al. (1998).

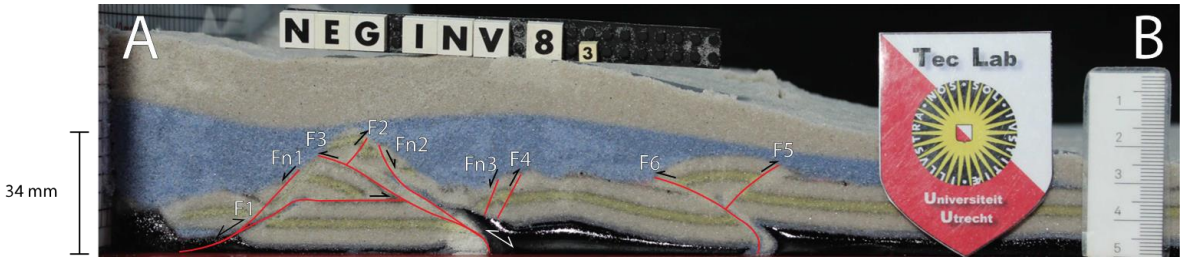

Figure 58: Cross sectional interpretation of cross section 3 through NEG INV 8.

The figure shows a structural interpretation on how the hanging wall of the system reacts to the extension. Combining the orientation and the geometry of the block-diagram, a similar structure is visible to what NEG INV 8 produced (Figure 58). The cross section of NEG INV 8 shows a structure that has many features in common. A low angle thrust that later has a higher angle normal fault that joins in on its plane at depth can be inferred in both instances (F1/Fn1 in NEG INV 8). Also, a low angle thrust that is (partly) reactivated and that has antithetic normal faults that terminate against the fault plane are visible in both instances (F3/Fn2 and Fn3 in NEG INV 8). These specific similarities indicate that the model behaves in a way that a natural area would in this tectonic setting and that the conclusion made from the experiments are transferrable to a natural setting. It also shows that the structures of NEG INV 9 and NEG INV 8 are relevant to natural structures.

This knowledge allows future field studies to make a first order approximation of the strength ratio in a system (i.e. “was this a high strength ratio decoupled system or a low strength ratio coupled system”). This can be done by comparing the geometry of the structures in the field to the high strength ratio system (NEG INV 8; D’Agostino et al. (1998)) and a low strength ratio tilted system (NEG INV 9; Ustaszewski et al. (2010)).

4.5. Future research

Future studies that aim to investigate similar topics using a similar set up should consider exclusively modelling brittle/ductile systems. These systems produce the most interesting and valuable results. Additional influences of e.g. strain rate, thickness variations and/or multi-layered rheological differences (i.e. multiple weak layers in the model, with stronger layers in between) can be explored.
The experimental set up presented in this thesis can be used as is, when further exploring. When it is wished to improve on the set up, a good starting point is to find a way to eliminate the perpendicular contraction of the rubber sheet during extension. This would result in much more usable data being produced per model compared to this thesis where realistically often only one cross sections can be interpreted per model. This increase in efficiency allows for more data to be produced in much less time, which was one of the largest hurdles for this thesis.

5. CONCLUSIONS

- A weak zone located along a thrust structure in a brittle/ductile regime causes reactivation to occur along (part of) that thrust structure during extension.
- In brittle only regimes, thrust structures are more likely to be extensionally reactivated in a distributed wedge. Yet only during the initial phase of extension and only little amounts. This indicates that for a brief period of time, it is favourable to reactivate the tectonic contacts over forming new faults.
- In brittle regimes with lower basal friction areas shortening occurs along a stratigraphic contact and the thrust structures are not reactivated during extension.
- Introducing tilt to the system localizes deformation (series i: 47% decrease, series ii: 22% decrease, series iii: 5% decrease) as the normal force of the base when pushing up a hill increases, increasing the basal friction of the base. Increased basal friction localizes deformation as shown by the experiments and by e.g. Brun et al. (2016).
- A higher coupled brittle/ductile negative inversion model has more distributed deformation (23% wider deformation zone).
- Brittle/ductile regimes accommodate extension by high amounts of shearing/stretching/thinning in the ductile part that are not associated with the main structures.
- Domains with ductile decollements will rotate forward thrusts to become steeper as a result of significant reactivation of back thrusts. This reactivation causes large blocks to slide down the contacts, rotating them in the process. Frictional decollement system will flatten forward thrusts during extension as no contacts are significantly reactivated, resulting in rotation.
- The experimental set up produces results that are comparable to natural examples of a thrust wedge located in a negative inversion tectonic setting (e.g. the Dinarides; Ustaszewski et al. (2010) and the Appenines; D'Agostino et al. (1998)).
- Particle analysis by using PIVlab is a critical tool in observing reactivational behaviour of structures. It allows the spectator to see significant reactivation that is not visible by looking at the markers in the cross sections.

6. ACKNOWLEDGEMENTS

I would like to thank Ernst Willingshofer and Kristóf Porkoláb for their constructive and timely feedback and for the numerous discussions we had. Their insights were very valuable in properly developing the experimental set up and in interpreting the results. Furthermore I would like to thank Ernst Willingshofer and the Tectonics group for the opportunity of performing this research with all the materials and machines available in the TecLab at the Utrecht University.

7. REFERENCES

Bonev, N., & Beccaletto, L. (2007). From syn- to post-orogenic Tertiary extension in the north Aegean region: constraints on the kinematics in the eastern Rhodope–Thrace, Bulgaria–Greece and the Biga Peninsula, NW Turkey. *Geological Society, London, Special Publications*, *291*(1), 113–142. https://doi.org/10.1144/sp291.6

Bonini, M., Sani, F., & Antonielli, B. (2012). Basin inversion and contractional reactivation of inherited normal faults: A review based on previous and new experimental models. *Tectonophysics*, *522–523*, 55–88. https://doi.org/10.1016/j.tecto.2011.11.014

Brun, J.-P. (2002). Deformation of the continental lithosphere: Insights from brittle-ductile models. *Geological Society, London, Special Publications*, *200*(1), 355–370. https://doi.org/10.1144/GSL.SP.2001.200.01.20

Brun, J., Faccenna, C., Gueydan, F., Sokoutis, D., Philippon, M., Kydonakis, K., & Gorini, C. (2016). The two-stage Aegean extension, from localized to distributed, a result of slab rollback acceleration. *Can. J. Earth Sci.*, *53*, 1142–1157.

Brun, J. P., & Faccenna, C. (2008). Exhumation of high-pressure rocks driven by slab rollback. *Earth and Planetary Science Letters*, *272*(1–2), 1–7. https://doi.org/10.1016/j.epsl.2008.02.038

Byerlee, J. (1978). Friction of Rocks. *Pure and Applied Geophysics*, *116*(4), 615–626.

Cooper, M. a, Williams, G. D., Graciansky, P. C. De, Murphy, R. W., Needham, T., Paor, D. De, … Williams, G. D. (1989). Inversion tectonics - a discussion. *Geological Society Special Publications - Inversion Tectonics*, (44), 335–347.

D'Agostino, N., Chamot-Rooke, N., Funiciello, R., Jolivet, L., & Speranza, F. (1998). The role of pre-existing thrust faults and topography on the styles of extension in the Gran Sasso range (central Italy). *Tectonophysics*, *292*(3–4), 229–254. https://doi.org/10.1016/S0040-1951(98)00070-5

Davis, D. (1983). Mechanics of fold-and- thrust belts and accretionary wedges. *Journal of Geophysical Research*, *88*(B2), 1153–1172. https://doi.org/10.1029/JB088iB02p01153

Ellis, S., Schreurs, G., & Panien, M. (2004). Comparisons between analogue and numerical models of thrust wedge development. *Journal of Structural Geology*, *26*(9), 1659–1675. https://doi.org/10.1016/j.jsg.2004.02.012

Faccenna, C., Nalpas, T., Brun, J.-P., Davy, P., & Bosi, V. (1995). The influence of pre-existing thrust faults on normal fault geometry in nature and in experiments. *Journal of Structural Geology*, *17*(8), 1139–1149. https://doi.org/10.1016/0191-8141(95)00008-2

Goetze, C., & Evans, B. (1979). Stress and temperature in the bending lithosphere as constrained by experimental rock mechanics. *Geophysical Journal of the Royal Astronomical Society*, *59*(3), 463–478. https://doi.org/10.1111/j.1365-246X.1979.tb02567.x

Hu, M., Li, S., Guo, L., Dai, L., Suo, Y., Somerville, I., … Ma, F. (2017). Dynamic mechanism of tectonic inversion and implications for oil-gas accumulation in the Xihu Sag, East China Sea Shelf Basin: Insights from numerical modelling. *Geological Journal*, *53*(May 2017), 225–239. https://doi.org/10.1002/gj.3044

Hubbert, M. K. (1937). Theory of scale models as applied to the study of geologic structures. *Geological Society of America Bulletin*, *48*(10), 1459–1520. https://doi.org/10.1130/GSAB-48-1459

Huet, B., Le Pourhiet, L., Labrousse, L., Burov, E., & Jolivet, L. (2011). Post-orogenic extension and metamorphic core complexes in a heterogeneous crust: The role of crustal layering inherited from collision. Application to the Cyclades (Aegean domain). *Geophysical Journal International*, *184*(2), 611–625. https://doi.org/10.1111/j.1365-246X.2010.04849.x

Klinkmüller, M., Schreurs, G., Rosenau, M., & Kemnitz, H. (2016). Properties of granular analogue model materials: A community wide survey. *Tectonophysics*, *684*, 23–38. https://doi.org/10.1016/j.tecto.2016.01.017

Krantz, R. W. (1991). *Normal fault geometry and fault reactivation in tectonic inversion experiments*. (56), 219–229.

McClay, K. R. (1989). Analogue models of inversion tectonics. *Geological Society, London, Special Publications*, *44*(1), 41–59. https://doi.org/10.1144/gsl.sp.1989.044.01.04

Porkoláb, K., Willingshofer, E., Sokoutis, D., Creton, I., Kostopoulos, D., & Wijbrans, J. (2019). Cretaceous-Paleogene Tectonics of the Pelagonian Zone: Inferences From Skopelos Island (Greece). *Tectonics*, (May). https://doi.org/10.1029/2018TC005331

Rosas, F. M., Duarte, J. C., Almeida, P., Schellart, W. P., Riel, N., & Terrinha, P. (2017). Analogue modelling of thrust systems: Passive vs. active hanging wall strain accommodation and sharp vs. smooth fault-ramp geometries. *Journal of Structural Geology*, *99*, 45–69. https://doi.org/10.1016/j.jsg.2017.05.002

Rudolf, M., Boutelier, D., Rosenau, M., Schreurs, G., & Oncken, O. (2016). Rheological benchmark of silicone oils used for analog modeling of short- and long-term lithospheric deformation. *Tectonophysics*, *684*, 12–22. https://doi.org/10.1016/j.tecto.2015.11.028

Schellart, W. P., & Strak, V. (2016). A review of analogue modelling of geodynamic processes: Approaches, scaling, materials and quantification, with an application to subduction experiments. *Journal of Geodynamics*, *100*, 7–32. https://doi.org/10.1016/j.jog.2016.03.009

Sibson, R. H. (1985). A note on fault reactivation. *Journal of Structural Geology*, *7*(6), 751–754.

Stojadinovic, U., Matenco, L., Andriessen, P. A. M., Toljić, M., & Foeken, J. P. T. (2013). The balance between orogenic building and subsequent extension during the tertiary evolution of the NE dinarides: Constraints from low-temperature thermochronology. *Global and Planetary Change*, *103*(1), 19–38. https://doi.org/10.1016/j.gloplacha.2012.08.004

Thielicke, W., & Stamhuis, E. J. (2014). PIVlab – Towards User-friendly, Affordable and Accurate Digital Particle Image Velocimetry in MATLAB. *Journal of Open Research Software, 2(1)*, (e30). https://doi.org/10.5334/jors.bl

Ustaszewski, K., Kounov, A., Schmid, S. M., Schaltegger, U., Krenn, E., Frank, W., & Fügenschuh, B. (2010). Evolution of

the Adria-Europe plate boundary in the northern Dinarides: From continent-continent collision to back-arc extension. *Tectonics*, *29*(6). https://doi.org/10.1029/2010TC002668

van Unen, M., Matenco, L., Nader, F. H., Darnault, R., Mandic, O., & Demir, V. (2019). Kinematics of Foreland-Vergent Crustal Accretion: Inferences From the Dinarides Evolution. *Tectonics*, *38*(1), 49–76. https://doi.org/10.1029/2018TC005066

Ventisette, C. Del, Montanari, D., Sani, F., & Bonini, M. (2006). Basin inversion and fault reactivation in laboratory experiment. *Journal of Structural Geology*, *29*(8), 1414–1416. https://doi.org/10.1016/j.jsg.2007.05.002

Vissers, R., Platt, J., & van der Wal, D. (1995). Late orogenic extension of the Betic Cordillera and the Alboran Domain: A lithospheric. *Tectonics*, *14*(4), 786–803. https://doi.org/10.1029/95TC00086

Wang, Q., Li, S., Guo, L., Suo, Y., & Dai, L. (2017). Analogue modelling and mechanism of tectonic inversion of the Xihu Sag, East China Sea Shelf Basin. *Journal of Asian Earth Sciences*, *139*, 129–141. https://doi.org/10.1016/j.jseaes.2017.01.026

Willingshofer, E., Sokoutis, D., Beekman, F., Schönebeck, J.-M., Warsitzka, M., & Rosenau, M. (2018). Ring shear test data of feldspar sand and quartz sand used in the Tectonic Laboratory (TecLab) at Utrecht University for experimental Earth Science applications. *GFZ Data Services*, (Figure 1), 1–12. https://doi.org/10.5880/fidgeo.2018.072

8. APPENDIX

8.1. Developing the set up

Part of this research project is designing and developing this experimental technique. For these experiments, using the available tools and materials, the set up presented above is the best working set up. A few technical pointers will be explained here, in case future studies wish to make use of this (or a similar) set up.

It is critically important that the distribution of force occurs over the entire width of the rubber sheet. For this set up this is achieved by clamping the rubber between aluminium bars using wood clamps (see image below).

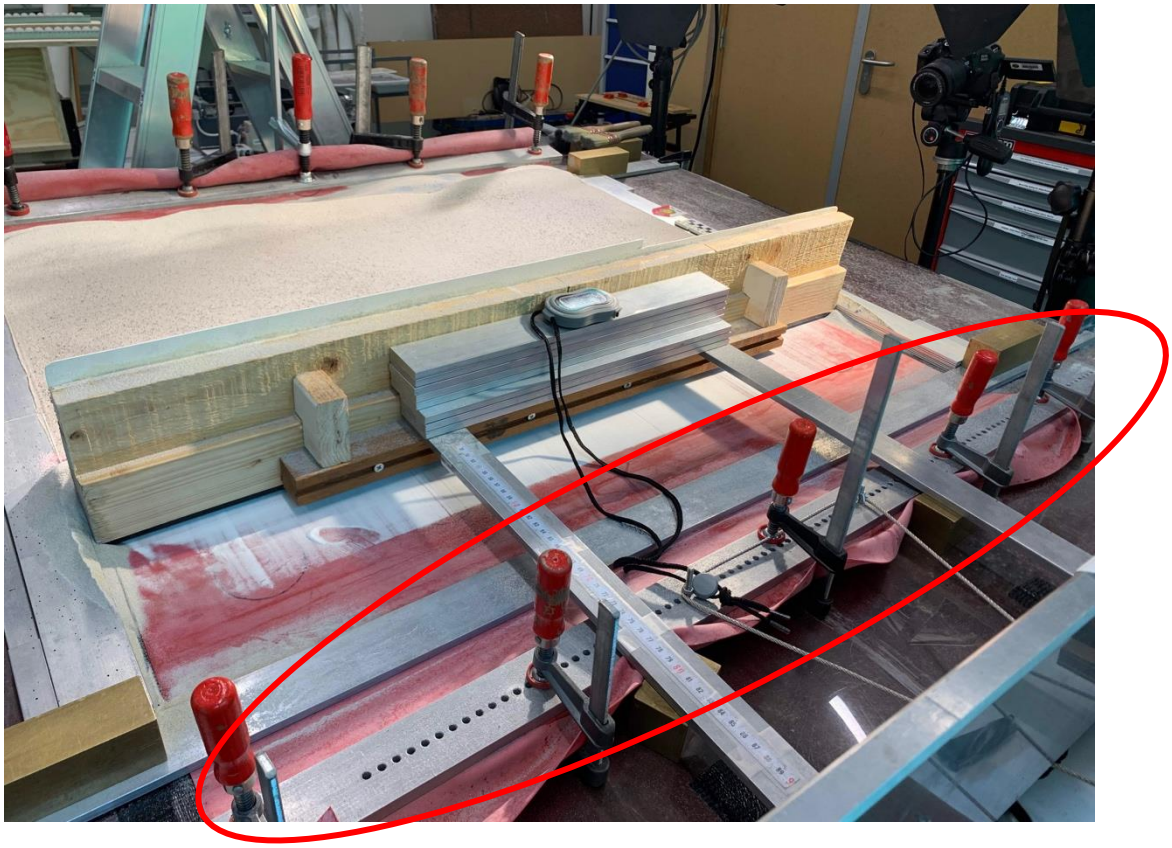

It is important to use enough clamps, otherwise the rubber will start to stretch differently over the length between clamps. In this set up a steel wire is passed through the clamps, as low to the table as possible. This wire is then attached to the engine. On the opposite side of the engine, the wire is first directed under the table using a set of pulleys. This allows the rubber to be stretched from both sides, using the same engine.
During extension the rubber tends to want to lift from the table. This is mitigated by passing the rubber sheet under two bars that pass over the entire width of the table. One bar at each side, right in front of the clamped ends (see image below, where one of these bars is shown).

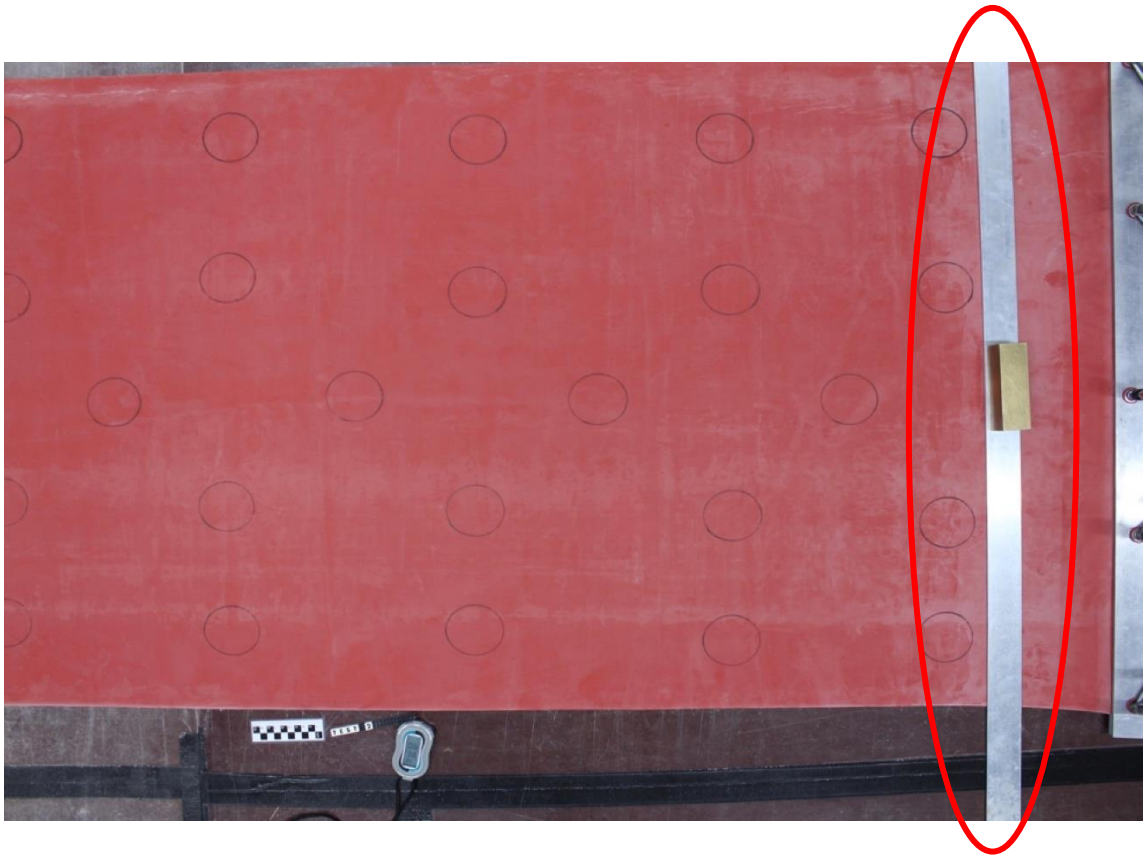

The use of steel wire is very deliberate as it has no stretching capabilities. Tests were done using highly non stretchable rope, yet this proved unusable due to excessive stretching.
An important note to the future use of a rubber sheet is that once silicone putty has been placed on the rubber, it is impossible to completely remove it. Be sure to run all experiments that do not use silicone putty on a clean, unaffected rubber sheet. This is also done during this research.
Some experiments aim to investigate the effects of introducing a 5º tilt to the system. This tilt is achieved by simply placing the legs of the table on one end on blocks. This inclination effectively increases the angle of the thrust faults during extension, which increases the likelihood of extensional reactivation (Faccenna et al., 1995) (see image below).

In total 17 test experiments were run. A short overview is given below.

Experiment	Objective
Test 1	Test clamping of rubber
Test 2	Modify and retest
Test 3	Modify and retest
Test 4	Try new clamping method
Test 5	Test new size rubber sheet
Test 6	First test with qtz. Testing how long until conjugate faults develop
Test 7	Test development of conjugate faults and boundary bars
Test 8	Test new removable backstop
Test 9	Trying to increase wedge size by inreasing amount of shortening
Test 10	Re-evalute the development of conjugate faults
Test 11	Test increased amounts of shortening
COMP ONLY [HF]	Test compression only with qtz as basal material
COMP ONLY [HF] 2	Test compression only with qtz as basal material with a slighly larger proto-wedge
COMP ONLY w/ TALC	Testing compression only with talc as low friction basal material
COMP ONLY w/ TALC 2	Testing compression only with increased shortening using talc
COMP ONLY w/ TALC 3	Re-test increased amounts shortening using talc
COMP ONLY w/ GB	Test compression only with glass beads as low friction basal material

The experiments above lead to the conclusion that with the current set up, 15 cm of shortening and 12 cm of extension are the maximum achievable results. The tests also concluded that glass beads are a better low friction basal material than talc when used on a rubber sheet.